Nanoscale

REVIEW

View Article Online
View Journal | View Issue

Cite this: *Nanoscale*, 2023, **15**, 2488

Recent progress on the synthesis of metal alloy nanowires as electrocatalysts

Shumin Li, Hui Jin and Yawen Wang *

Received 31st October 2022,
Accepted 30th December 2022

DOI: 10.1039/d2nr06090f

rsc.li/nanoscale

Benefiting from both one-dimensional (1D) morphology and alloy composition, metal alloy nanowires have been exploited as advanced electrocatalysts in various electrochemical processes. In this review, the synthesis approaches for metal alloy nanowires are classified into two categories: direct syntheses and syntheses based on preformed 1D nanostructures. Ligand systems that are of critical importance to the formation of alloy nanowires are summarized and reviewed, together with the strategies imposed to achieve the co-reduction of different metals. Meanwhile, different scenarios that form alloy nanowires from pre-synthesized 1D nanostructures are compared and contrasted. In addition, the characterization and electrocatalytic applications of metal alloy nanowires are briefly discussed.

1. Introduction

Developing sustainable energy harvesting and storage methods to reduce or replace fossil fuel usage has become one of the most focused-on research areas in recent years.[1–5] Overcoming the low kinetics of many important electrochemical processes is of critical importance for the application and commercialization of future techniques, such as fuel cells that directly convert chemical energy to electrical energy, the water-splitting process that produces H_2 as clean energy sources, and the CO_2 reduction and conversion devices that help to reduce the greenhouse gas level in the atmosphere and produce functional carbonaceous products.[6–13] Catalysts are indispensable for achieving this, and thus significant amounts of research have been devoted to developing catalysts with high activity and durability.[14–24]

The performances of the catalysts can be improved by optimizing the morphology, composition, and other structural properties of the materials.[18,25,26] The adsorption and desorption of the reactants and intermediates on the surface of the catalysts depend directly on the amount of active sites and the adsorption energy at these sites, which is in turn determined by the shapes and surface structures of the catalysts.[15]

The unique structural characteristics of one-dimensional (1D) nanostructures, or nanowires, give rise to multiple advantages in catalytic reactions, as recently summarized in several comprehensive review works.[25–34] Firstly, the nanowires with high aspect ratio have enormous surface areas that can provide a large number of active sites for electrochemical reactions.[27,32,33] Although geometrically, the surface area of

Institute of Advanced Synthesis (IAS), Chemistry and Molecular Engineering, Nanjing Tech University, Nanjing 211816, P.R. China. E-mail: ias_ywwang@njtech.edu.cn

Shumin Li

Shumin Li is currently a graduate student at Nanjing Tech University. She received her B.S. degree in applied chemistry from Shaanxi University of Technology in 2020, and has since been working with Prof. Yawen Wang in the synthesis of one dimensional nanomaterial.

Hui Jin

Hui Jin is a graduate student at Nanjing Tech University. He obtained his B. S. degree in chemical engineering from Shanxi Datong University in 2020, and has since been working in Prof. Yawen Wang's group to study the synthesis and electrochemistry of nanowires.

the nanowires is smaller than the same volume of nanoparticles with the same diameters, in practice they may still have more exposed surface areas during the electrochemical processes, as nanoparticles are more vulnerable to aggregation during the catalyst loading and cycling processes.[30,31] This also give rise to the second advantage of nanowires: they usually have better structural stability, being more resistant to dissolution, aggregation and Ostwald ripening, and thus show improved durability in catalytic reactions.[30] The linear elongation of nanowires is also considered to provide electron highways for charge transportation and diffusion tunnels for mass transportation, and both are beneficial for catalytic activity.[27,29] Lastly, nanowires are readily assembled into free-standing 2D films or 3D networks, which are more easily processed into electrodes in devices.[31]

On the other hand, the formation of the metal alloy provides an additional dimension to modify the chemical and physical properties of catalytic nanomaterials. Recently, the exploration of 1D nanostructure catalysts has gradually extended from pristine metal nanowires to multi-metal alloys.[25,32]

One major benefit of forming an alloy is to provide adjustment of the surface electronic structures of the catalysts, leading to optimized binding between the catalyst surfaces and key intermediates of the electrocatalytic reactions.[35–38] For example, metals have different adsorption energies towards the *OH species, which is the key intermediate during oxygen reduction reactions (ORRs).[36,39] And although Pt and Pd are the best ORR catalyst candidates, the adsorption energies of *OH on these metals are still not optimized according to the volcano plot.[36,40] Forming alloys inevitably leads to electron transfer between the different metals. In addition, the introduction of foreign metal would alter the bond lengths of the metallic crystals. These effects would cause change in the electron density on both elements, causing variation of the adsorption energies of the reaction intermediates.

Moreover, there are also synergistic ensemble effects between the metal compositions. For example, the AuCu surface would have increased selectivity for C–C formation in the CO_2 reduction reaction (CO_2RR), as the Au atoms around the Cu could provide addition binding sites for the *COOH intermediates.[41] Also, the Pd-M alloy has a lower risk of being poisoned by CO, as the CO_{ad} only adsorbs on the adjacent Pd atoms.[42] The Pd-M alloy surface, with Pd more diluted on the surface compared with pure Pd, is thus more preferred in processes such as formic acid oxidation.

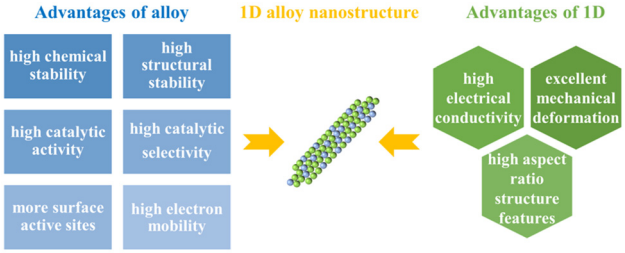

Fig. 1 Schematics illustrating the advantages of 1D metal alloy nanostructures.

Combining both the advantages of 1D nanostructures and alloy materials, metal alloy nanowires are thus promising electrocatalyst candidates (Fig. 1). On one hand, this group of material inherits the structural advantage of 1D nanostructures, possessing a large number of surface active sites, high structural stability, and high electron mobility during electrochemical processes.[34,43] On the other hand, the intrinsic catalytic activity of the material could be further enhanced by adjustment of the compositions.[44,45] For instance, Ni and/or Co were often incorporated into Pt and Pd to from alloy nanowires with improved ORR performances. Other metals, such as Au, Ag, Cu, Rh, Ru, Zn, Ir, Pb and Fe *etc.* are also common metal compositions in alloy nanowires.

Synthesis is of fundamental importance in the exploration of advanced functional materials. Many works about alloy nanowires have emerged recently, and the electrocatalytic performances of these materials have been studied thoroughly. In this work, the synthetic approaches, mostly solution-based chemical methods, for different metal alloy nanowires are reviewed and categorized. 1D nanostructures with imperfect wire-like morphologies, such as chain-like nanostructures and branched nanowire networks, are also included as they are sometimes considered as nanowires and possess similar structural advantages. While some of the syntheses and applications of Pt and Pd-based nanowires have been separately reviewed in recent review works, this work aims to systematically discuss the mechanism for obtaining 1D structures, the various synthetic approaches that are used to enable the formation of the alloys, and the recently developed strategies that advance the synthetic capabilities. To better illustrate syntheses, the common characterizations for metal alloy nanowires are first introduced. In addition, the applications of metal alloy nanowires as electrocatalysts are also briefly summarized to demonstrate the advantage of this group of materials.

Yawen Wang

Dr Yawen Wang is currently a professor in the School of Chemical and Molecular Engineering at Nanjing Tech University in China. She obtained her B. Sc. (2010) and Ph. D. (2015) degrees from Nanyang Technological University in Singapore, and worked there as postdoctoral research fellow before joining Nanjing Tech University in 2017. Her research focuses mainly on the controlled synthesis of nanomaterials, especially the synthetic mechanism and catalytic application of the low-dimensional metal nanostructures.

2. Characterization of metal alloy nanowires

Characterizations are vital for synthetic works, and they also provide clues for mechanism studies and discussions about structure–property co-relationships. For metal alloy nanowires, both the structures and the compositions of the synthetic products need to be well characterized, and the structural aspect includes both the morphological shapes and crystalline structures of the materials.

The morphology of the 1D nanostructures can be confirmed easily with microscopic methods, including most commonly transmission electron microscopy (TEM) and scanning electron microscopy (SEM). Often, either TEM or SEM would be necessary to indicate the morphology of the nanowires, yet both can be used to give better illustrations, including the topology of nanowires with rough surfaces as well as possible porous structures. However, although almost all syntheses would allow microscopic characterizations, it should be noted that these methods can only provide information for a tiny portion of the product obtained from the synthesis. Low magnification images that contain sufficient numbers of the nanowires should be provided to verify the uniformity of the synthesis.

Another key issue that has often been overlooked is that microscopic methods are off-line characterizations that show only the appearance of the species on the specimen. The dried sample may undergo transformations when loaded to the sample holder and subjected to vacuum for electron microscopic characterizations. Therefore, although most works have interpreted growth mechanisms based on TEM images of the intermediates at various reaction stages, the possibility of deviation of the characterization results from the solution situations in reality needs to be considered when constructing the synthesis mechanisms. Control experiments are highly desirable to confirm the hypotheses in addition to the characterization results.

The crystalline structures of metal alloy nanowires are usually characterized with high-resolution TEM techniques (HRTEM) and diffraction techniques such as X-ray diffraction (XRD) and selected area electron diffraction (SAED). The former provides the d spaces value of some low index facets of a small portion of the samples, while the diffraction methods give the ensemble properties. It should be noted that ultrathin metal nanowire may suffer beam damage and undergo lattice transformations when under high energy electron beams during the HRTEM characterizations,[46] bringing ambiguities to the structure discussions. Additionally, surface organic ligands may blur the images during the characterization after being reduced by the electron beam and accumulated on the surface of the nanowires. Therefore, the acceleration voltage of the electron beam may need to be lowered and the nanowires' surface may need to be cleaned to remove organic ligands before HRTEM characterizations.

The composition of metal alloy nanowires takes much more effort to be characterized. Given the small diameters of most nanowires, the distribution of the metals is usually characterized with energy-dispersive X-ray spectroscopy (EDS) coupled with high-angle annular dark field scanning transmission electron microscopy (HAADF-STEM). EDS mapping can give the distribution of the various elements across the nanowires. Again, for ultrathin nanowires, the mapping process would be much more difficult, as the low quantity of metal materials would require repeated scans and thus prolonged scanning times, adding to the risk of being affected by image shifting, vibration and possible damage from the beam. Even with prolonged scan durations, EDS mapping may not provide atomic resolution. Therefore, characterization of the atomic distribution of the different elements remains a great challenge. On the other hand, HAADF-STEM, which characterizes the Z contrast of the samples, can provide certain information about the nanowires' composition.[47] It generates intensity profiles that can be used to establish the features of the element distributions, especially with the aberration-corrected high-resolution HAADF-STEM which can provide atomic-scale images.

Apart from the microscopic methods, powder XRD results are often used as evidence to illustrate the formation of alloy. Deviations of the XRD peaks from the pristine metal phases due to shrinking or expansion of the lattice structures is usually attributed to the incorporation of a foreign metal with different crystalline constant.[48,49] A typical bimetallic alloy would have peaks occurring in between those of the two pristine metals, unless a certain alloy phase was generated. In addition, the width of the XRD peaks can be used to estimate the grain sizes in the nanowires.

The electronic structures of the metals in an alloy are often characterized with X-ray photoelectron spectroscopy (XPS) methods, which also help to confirm the existence of certain elements. The change of binding energies in XPS spectra can be explained by electron transfer between the metals in the alloy. Thus the XPS results are strong evidence for the formation of the alloy structures, and also can provide clues to explain the change of catalytic activity of the alloy nanowires.

Apart from the usual characterizations, recently the X-ray absorption spectroscopy (XAS) methods X-ray absorption near-edge structure (XANES) and extended X-ray absorption fine structure (EXAFS) have been employed to investigate the atomic and electronic structures of the metals in alloy nanowires.[50] XANES can precisely characterize the oxidation state of the metals. The XANES edges change in intensity and position if the oxidation state of the target metal varies. And the oxidation state of the sample can be confirmed by comparing the spectra with those of compounds with known oxidation states. For instance, the XANES of the three elements in the PtNiMo nanowires were compared and contrasted with pristine metal foils and a few common compounds (Fig. 2a, c and e).[51] In particular, the shoulder peak in the XANES feature of Mo suggests that some of the Mo in the alloy nanowires is similar to that in MoO_3. The EXAFS method provides complementary information about the local atomic structures. The EXAFS signals are oscillations of the wave of the ejected photoelectron scattered by the surrounding atoms. Both the distances and types of the surrounding atoms affect the EXAFS spectrum, therefore it can also give the fine structures of the alloy nano-

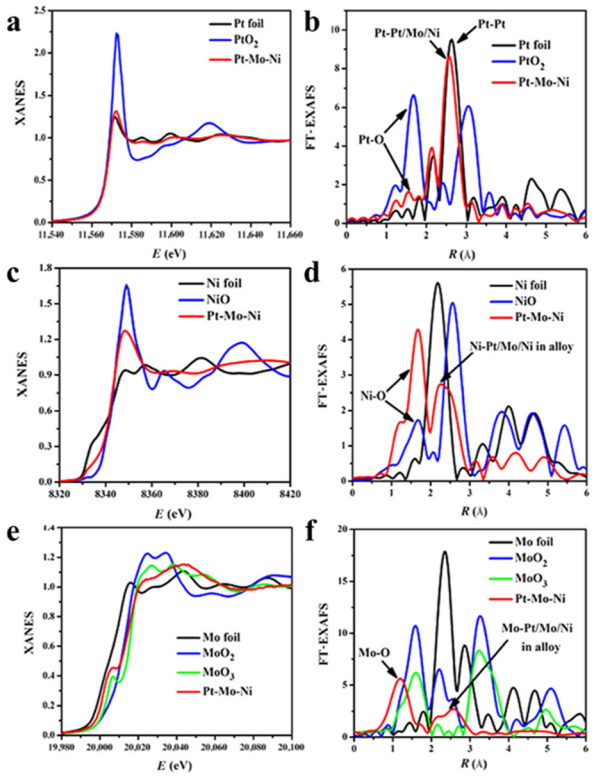

Fig. 2 XAS analyses of the PtMoNi NWs. XANES (a) and EXAFS (b) analysis of Pt L_3-edge (FT range, 4.3 to 14.5 $Å^{-1}$). XANES (c) and EXAFS (d) analysis of Ni K-edge (FT range, 2.5 to 12.5 $Å^{-1}$). XANES (e) and EXAFS (f) analysis of Mo K-edge (FT range, 2.0 to 10.5 $Å^{-1}$). Reprinted with permission from ref. 51. Copyright 2017 from AAAS.

wires. Again by comparing the EXAFS spectra with references, typical interactions can be assigned (Fig. 2b, d, and f). For instance, the EXAFS spectra of Ni indicate that there are two Ni species in PtNiMo alloy nanowires: NiO as indicated by the scattering between 1.5 and 2.0 Å, and metallic Ni in the PtNiMo alloy. The peak between 2.0 and 2.9 Å was probably the combination of both the Ni–Ni scattering in NiO and the Ni-metal scattering in the alloy.

Although the XAS methods can provide useful information on the fine structure of alloy nanowires, they have not been frequently used in the reported syntheses. One key issue is that they are synchrotron analyses that require the use of synchrotron radiation, which may not be available to many researchers. Similar issues also apply to the cutting-edge microscopic characterizations that provide atomic resolution on nanowire structures, as these methods require well-trained personnel to operate the instrument and interpret the results. Thus, interdisciplinary cooperation has become increasingly important and desirable in the related communities.

3. Direct synthesis of alloy nanowires

There are two major issues of concern in the synthesis of metal alloy nanowires: (1) how to induce the 1D growth of the metals, and (2) how to form the alloy with certain composition in a controlled manner.

Unlike intrinsically linear materials such as carbon nanotubes, metals have highly symmetric crystalline structures. Instead of elongating in two directions, the equivalent facets in metal crystals grow simultaneously to give 3D structures, unless the symmetry is broken with certain mechanisms. In bottom-up approaches, the crystalline symmetry can be broken with either templates, the oriented attachment mechanism, or kinetic-controlled growth induced by either defects or ligands.

Direct synthesis of metal alloy nanowires usually follows similar mechanisms that form pristine metal nanowires, but with simultaneous co-precipitation of all alloy compositions (Fig. 3). The synthesis of nanowire can be realized *via* either templating methods or self-assembly processes. Tubular hard templates can be used coupled with the deposition process to generate 1D nanostructures. And in solution, one or multiple structure-directing reagents, such as CTAC, CO and PVP, are usually required to induce the 1D growth of the metal nanostructures. Some of the structure-directing reagents are considered to form micellar-structures to induce the linear growth of the metals, while in some cases the exact mechanisms of the 1D growth have not been completely established yet.

For templating methods, overcoming the differences in the reduction potential of various metal precursors is the key issue for a successful co-precipitation process. In solution-based synthesis, one composition of the alloy nanowire is usually responsible for the morphological construction, serving as the "nanowire template". Pt or Pd is often the metal that plays this role, probably because the syntheses of the Pt and Pd nanowires are quite feasible compared with other nanowires. Nevertheless, those formed *via* a one-pot procedure and that have no obvious core–shell structures are still discussed in this section. Often, the chemical environments in direct syntheses allow the co-reduction or autocatalytic reduction of the precursors of the alloys, while sometimes synthetic adjustments are necessary to enable the co-precipitation processes. It is also

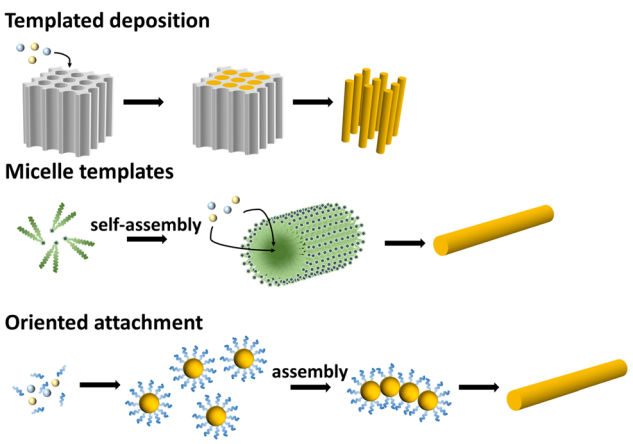

Fig. 3 Schematics illustrating the formation mechanisms that forms the metal alloy nanowires directly with chemical methods.

noticed that in some rare cases nanowires can only be obtained when there are two or more metal precursors, and no single-metal nanowires can be obtained.

3.1 Electrodeposition with hard templates

Hard templates have often been combined with electrodeposition to synthesize nanowires. This approach has been frequently used to obtain nanowires made of the magnetic metals, for instance the super invar (Fe–CO–Ni) alloy nanowire; it is difficult to reduce these metals in a wet-chemical environment, probably due to their relatively low reduction potentials compared with the noble metals.[52–56] One of the most widely applied templates for 1D electrodeposition is the anode-aluminum-oxide (AAO), which can be easily obtained by anodizing Al foil and removed after the synthesis with chemical etching. With the AAO template, a vertically aligned nanowire array can be electrodeposited, with the diameters of the nanowires determined by the pore sizes. Nanowires synthesized with this method usually have diameters of about the tens of nanometres.

Recently, there have been several works reporting the syntheses of Pd-based nanowires with the AAO-templated electrodeposition methods, including pure Pd and PdBi,[57] PdFe,[58] PdCo[59] and PdNi[56] nanowire arrays. The applied potentials often significantly affect the composition of the PdM alloy nanowires. This is because Pd can be deposited at relatively low overpotential, while the other metals need much negative potentials. The overall Pd compositions usually decrease with the increase of the applied potentials. Alternatively, the ratio of the precursors in the electrolyte can be adjusted to control the composition of the final nanowires. The removal step of the hard AAO template can offer an additional chance to tune the nanowire composition and modify the surface topology of the nanowires. For instance, PdBi nanowires with a rough surface can be generated during the etching of the AAO templates after depositing smooth PdBi nanowires in the template.[57] Meanwhile, the composition of Bi in the alloy also dropped from 15% to 3% due to the dissolution of the surface Bi (Fig. 4).

The templates in electrodeposition restrict the outlines of the nanowires, and the deposition conditions can provide extra controls on the morphologies of the alloy nanowires. A recent synthesis of FeCoNi nanowires carried out the deposition at low pH condition with polycarbonate as the template, and produced porous nanowires.[60] The H_2 bubbles formed during the electrodeposition were utilized as the dynamic templates of the pores in the alloy nanowires. Moreover, post-synthetic processing such as surface etching can be conducted to produce PdM nanowire arrays with rough or porous surfaces, and to further adjust the composition of the nanowires.[57,59]

Templated electrodeposition is a feasible method to synthesize metal alloy nanowires with both noble and non-noble metal compositions. The composition of the alloy nanowires is usually controlled by the reduction potentials. Both the surface morphology and compositions of the obtained nanowires can be further adjusted with post-synthetic treatments.

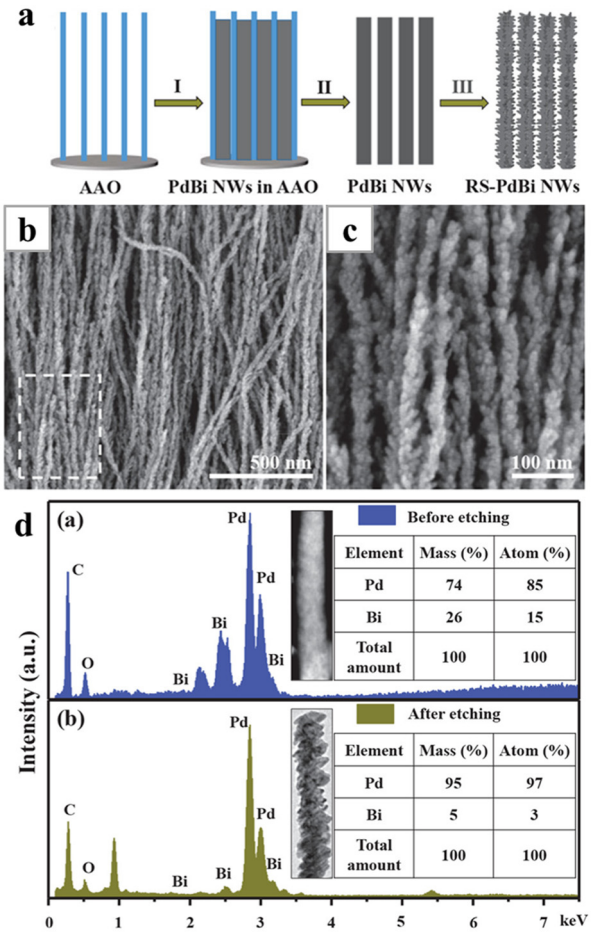

Fig. 4 (a) Schematics illustrating the electrodeposition process with AAO template; (b) SEM and (c) magnified SEM images of PdBi nanowires with rough surfaces. (d) EDS analysis results showing the compositions of PdBi nanowires before and after being etched in 4 M NaOH. Reprinted with permission from ref. 57. Copyright 2019 from American Chemical Society.

3.2 Solution-based synthesis with molecular ligands

Many metal-based nanowires have been synthesized *via* solution-based chemical methods. The homogeneous environment in wet-chemical synthesis can offer good structural uniformity and afford potentially massive production. During the syntheses, apart from the metal precursors and the reducing systems, one or more molecular structure-directing reagents or ligands, such as the organoammonium halides, organoamines, metal carbonyls which provide CO and/or non-ionic surfactants, are usually added as vital ingredients to induce the 1D growth of the metals. Normally, the ligands were considered as either promoting the oriented attachment of particle intermediates to form 1D assemblies, or forming micelle templates facilitating the 1D growth of the metal crystals. The exact mechanism of the 1D growth induced by some of the structure-directing reagents had been thoroughly studied, yet for some other ligands, it remains unclear how these species direct the linear growth of metal nanostructures.

3.2.1 Organoammonium halides-induced growth. Organoammonium halides have been widely employed in the synthesis of nanowires and nanorods.[61–64] The organoammonium halides with long carbon chains are amphiphilic, and they are believed to form tubular-like micelles that serve as soft templates. One widely applied solution-based system to synthesize Pt-based alloy nanowires employs the cetyltrimethylammonium (CTA^+) halides, typically cetyltrimethylammonium chloride (CTAC), as the structure-directing reagent, with metal acetylacetonate (acac) as the precursor, oleylamine as the solvent and glucose as the reductant. PtNi,[65–69] PtCo,[70,71] PtFe,[65,72] PtRh,[65] PtZn[73] and the ternary PtNiCo,[65] PtNiFe,[65] PtCoRh,[74] PtRuNi[75] alloy nanowires have been shown to be synthesized with the CTAC system (Fig. 5). The majority of these alloy nanowires possess a chain-like or zigzagging morphology, suggesting plausible similar formation mechanisms. In addition, Ga-doped Pt_3Co nanowires with a lavender morphology were obtained by introducing Ga $(acac)_2$ during the synthesis.[76] Sometimes, cetyltrimethylammonium bromide (CTAB) can be used to replace CTAC and obtain similar nanowire structures.[77] In some reported syntheses CTAB and CTAC were interchangeable, while in other works only one of them can induce the 1D growth. This ambiguity may be because the ligand not only directs the morphology of the nanostructure, but also greatly affects the reduction and deposition kinetics of the metals. More recently, subnanometer high-entropy-alloy (HEA) nanowires composed of more than five metals, the PtRuNiCoFeMo nanowires, were reported to be synthesized following a similar approach, with stearyltrimethylammoium bromide (STAB) as the surfactant.[78] While many HEA nanostructures have been obtained *via* high-temperature processes,[79,80] this work demonstrates the potential of the solution-based methods in the synthesis of complex alloys.

Mechanistic investigation of the formation of PtNi alloy nanowires indicated that during synthesis, Pt was first reduced and formed ultrathin nanowires, followed by the reduction of Ni and the formation of a core–shell intermediate.[65] As the reduction progressed further, an alloy process occurred and the interdiffusion of the metal atoms led to the formation of the alloy nanowires (Fig. 6). Moreover, the surface layer of the ultrathin nanowires was usually considered Pt-rich, as compared with Ni the Pt atoms would be chemically more stable and thus concentrated on the surface as the result of both the interdiffusion and ripening processes. Overall, this method relies greatly on the formation of the 1D Pt nanostructure. Without Pt, Ni alone could not have linear growth. Nevertheless, the interdiffusion of metal atoms at high temperatures is also of critical importance to the formation of uniform alloy phases, such as the Pt_3Ni alloy phase in PtNi alloy nanowires.

The sequential reduction of Pt and Ni suggests that the synthesis can be modified to two-step procedures, through which the phase and composition of the PtNi alloy nanowires can be adjusted more precisely. It was reported that varying the quantity of the $Ni(acac)_2$ added in the second step could lead to the formation of a series of Pt_3Ni, Pt_3Ni_3, $Pt_3Ni_{4.5}$ and Pt_3Ni_6 alloy nanowires, with the excess Ni forming a segregated Ni phase.[66] Further etching of the Ni phases with acetic acid led to the formation of a porous Pt_3Ni nanowire with improved electrocatalytic performance. Another recent work indicates that apart from crystallization during the synthesis process, post-synthetic thermal treatment under NH_3 atmosphere can also induce Ni segregation on the surface of the PtNi nanowires, as the Ni has stronger affinity towards NH_3 than Pt.[67]

The two-step procedure also provides means to form alloys with metals having large potential differences or reducing

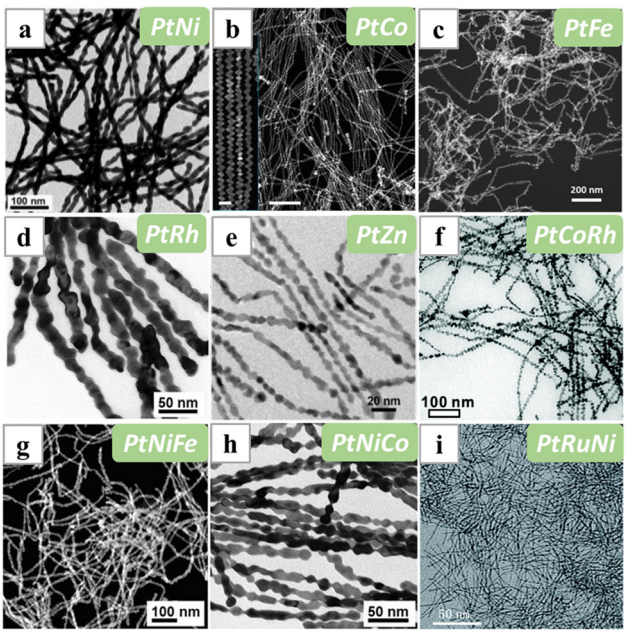

Fig. 5 TEM/STEM/HAADF-STEM images of (a) PtNi, (b) PtCo, (c) PtFe, (d) PtRh, (e) PtZn, (f) PtCoRh, (g) PtNiFe, (h) PtNiCo and (i) PtRuNi nanowires synthesized with CTAC as the structure-directing reagent. Reprinted with permission from ref. 65, 71–75. Copyright 2015 and 2018 from WILEY-VCH GmbH, 2016 and 2019 from Springer Nature, 2020 and 2021 from the Royal Society of Chemistry.

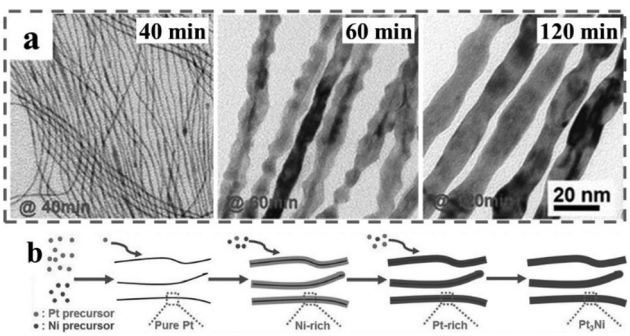

Fig. 6 (a) TEM images of 1D PtNi intermediates collected from the reactions at different reaction times during the CTAC-mediated synthesis of PtNi alloy nanowires. (b) Schematics illustrating the growth mechanism of 1D PtNi nanowires. Reprinted with permission from ref. 65. Copyright 2015 from WILEY-VCH GmbH.

kinetics with Pt, such as PtCu and PtCuIr, PtCuRh, PtCuPd nanowires.[81,82] Typically, the reaction mixture was first heated with solely the Pt precursor to generate ultrathin Pt nanowires, and then the precursors of the other metals were added together with additional Pt precursor to induce the formation of the alloy nanowires. The reduction temperature of the second stage can be increased to facilitate the reduction of the second metal. For instance, PtCoRh spiral nanowires could be obtained by first forming PtCo alloy nanowires at 130 °C, and then raising the reaction temperature to 170 °C to achieve the reduction and deposition of Rh.[74]

In this CTAX (X = Br or Cl)-induced synthesis, although the solvent oleylamine is reductive, additional reductant glucose was also added to promote the reduction of the metal with low reduction potential. In the absence of glucose, pure Pt nanowires were usually obtained. An exception is the formation of chain-like PtNi nanostructures under the solvothermal condition at 180 °C.[83] The high-temperature solvothermal condition probably maintained a highly reductive environment that allowed the reduction of Ni and the formation of Ni-rich nanospheres along the Pt nanowires. Other reductants have also been introduced. Replacing the glucose with ascorbic acid or citric acid during the synthesis of Pt_3Ni nanowires yielded sinuous nanowires or short nanorods, repectively.[84] These results verified that the reduction system also played an important role in the 1D growth, as the deposition of the metal atoms on certain surfaces of the nuclei was related closely to the adsorption/desorption kinetics of the ligand and the deposition kinetics of the metal. Alternatively, PtNiMo ultrathin nanowires were produced by purging pressurized H_2 (30 bar) into the nanowire growth system.[51] H_2 was considered as both controlling the slow kinetics for the growth of the nanowires and providing structural regulation for nanowire formation.

Carbonyl reagents, typically $Mo(CO)_6$[51] and $W(CO)_6$,[85,86] have been introduced into some of the syntheses, and their addition can cause the transformation of the nanowire morphology from chain-like to ultrathin. Upon heating, metal carbonyl decomposes to release CO, which adsorbs strongly on the Pt surface and provides restriction to the lateral growth of the nanowires. As a result, ultrathin Pt-based nanowires were obtained with the metal carbonyl additives. For instance, the length of the Pt_3Ni nanowire increased from 9 nm to about 35 nm when the mass of $Mo(CO)_6$ added into the system was doubled from 2 mg to 4 mg.[87] Moreover, the presence of CO was found to be critical for the smoothening of the nanowires after the oriented attachment process. Chain-like assembly of nanoparticles was obtained if there were no metal carbonyl additives during the synthesis (Fig. 7).[82] Alternatively, CO could be introduced to the system by directly blowing the reaction mixture with gaseous CO. After that, the autoclave containing $Pt(acac)_2$ and $Fe(acac)_2$ was sealed and heated under solvothermal condition to generate ultrathin PtFe nanowires.[88] Apart from morphological control, the introduction of CO also generates a highly reductive environment. Even without glucose, PtRu nanowires could still form in the presence of $W(CO)_6$, with dimethyldioctadecylammonium chloride as the ligand.[89]

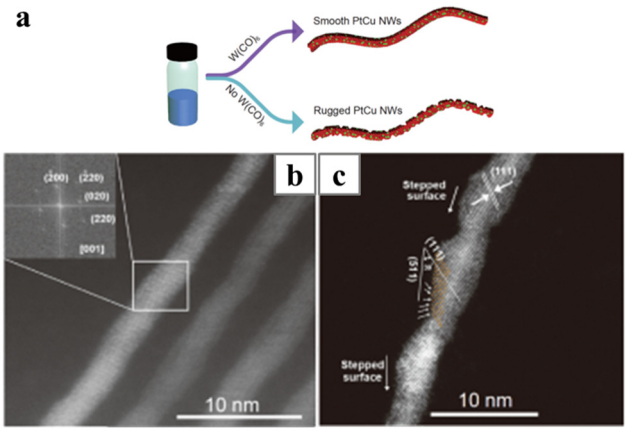

Fig. 7 (a) Schematics illustrating the effect on the $W(CO)_6$ on the surface of the PtCu nanowires and (b and c) HAADF-STEM images of (b) the smooth PtCu nanowires (inset showing the corresponding FFT pattern) and (c) the rugged PtCu nanowires. Reprinted with permission from ref. 82. Copyright 2020 from Springer Nature.

Another type of double-chain organo-ammonium halide has been employed in the growth of Pd-based alloy nanowires in aqueous solutions. A typical system carries the reaction in aqueous solution, with dioctadecyldimethylammonium chloride (DODAC)[90,91] as the structure-directing reagent and L-ascorbic acid as the reductant. The aqueous solution favours the usage of the L-ascorbic acid, while the hydrophobic carbonyl reagents are not compatible for this synthesis. More importantly, in aqueous solution the double-chain DODAC was considered to be a better ligand compared with the more commonly used CTAB and CTAC: the double-chain organo-ammonium halide can form stable tubular mesophases in the aqueous solution, providing stable soft templates for the formation of single-crystalline Pd nanowires (Fig. 8).[92] Simply by reducing $AgNO_3$ or H_2PtCl_6 together with H_2PdCl_4, alloys PdAg and PdPt nanowires can be obtained. One variation of this system was the introduction of NaH_2PO_2 as the reductant to replace the ascorbic acid. NaH_2PO_2 also provides P during the reduction, leading to the formation of PdCuP alloy nanowires.[93] Recently, a similar molecule, dihexadecyldimethylammonium chloride (DHDAC) has been employed as the structure-directing reagent to synthesize ultrathin PdAg nanowires.[94] The ratio of Pd and Ag in the alloy nanowire was consistent with the ratio of the metal precursors. Interestingly, this system is incapable of forming pure metal nanowires. When solely Pd or Ag precursor was used, Pd or Ag nanoparticles were obtained.

Besides the ammonium halides, hexadecylpyridinium chloride (C_{16}-py) was also recently discovered to be capable of forming micelle-like soft templates for the synthesis of 1D Pd-based nanostructures. The amphiphilic ligand first assembled with the Pd precursor and formed columnar structures. After adding H_3BO_3 and dimethylamine borane (DMAB), PdB nanoparticles nucleated inside the columnar structures. Finally, the nanoparticles attached together to generate wavy PdB and PdMB (M = Cu, Pt) nanowires.[95]

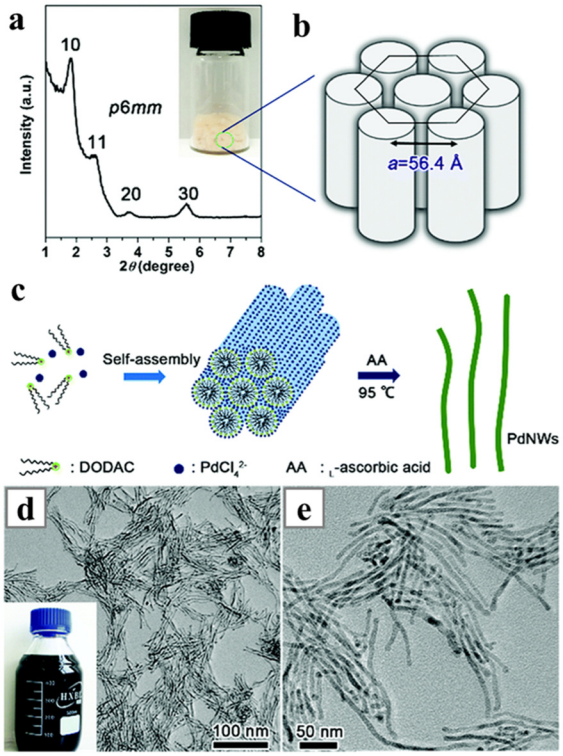

Fig. 8 Synthesis of the Pd nanowires with DODAC. (a) Small-angle XRD patterns of the powder mainly consisting of DODAC and H_2PdCl_4, with the inset showing the photograph of the spongy powder in a glass bottle. (b) Structural representation of a characteristic *p6mm* mesostructure. (c) Proposed formation mechanism of Pd nanowires based on a self-assembly process. (d and e) TEM images of the Pd nanowires observed at different magnifications. Reprinted with permission from ref. 92. Copyright 2016 from the Royal Society of Chemistry.

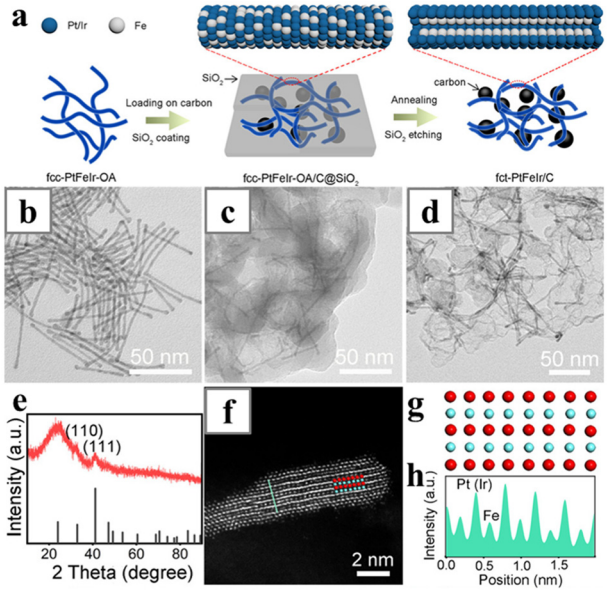

Fig. 9 Synthesis of fct-PtFeIr/C *via* a silica-protected annealing strategy. (a) Schematics illustrating the synthesis process. (b–d) TEM images of (b) fcc-phase PtFeIr nanowires, (c) fcc-PtFeIr-OA/C@SiO_2, and (d) fct-PtFeIr/C. (e) XRD pattern of the fct-PtFeIr/C. (f) HAADF-STEM image of a nanowire in fct-PtFeIr/C viewed along the [100] axis. Red and cyan spheres represent Pt (Ir) and Fe, respectively. (g) Simulated atomic arrangement for fct-phase PtFe viewed along the [100] axis. (h) *Z*-Contrast intensity profile taken along the cyan line in (f). Reprinted with permission from ref. 100. Copyright 2021 from Wiley-VCH GmbH.

3.2.2 Metal carbonyl-induced synthesis. As mentioned above, CO has often been introduced in the form of metal carbonyl together with structure-directing ammonium halide to promote the elongation of Pt-based ultrathin nanowires. Alternatively, metal carbonyls alone have been shown capable of inducing the formation of PtFe,[96,97] PtCo,[97] PtCoFe[98] and PtFeNi[99] alloy nanowires. Organic solvents with high boiling points were usually used in these systems, as metal carbonyls are soluble in these solvents and their decomposition requires high temperatures. In a typical synthesis, $Pt(acac)_2$, $Fe(CO)_5$ or $Co_2(CO)_8$ and oleylamine were mixed with octadecene solution containing sodium oleate and heated to 240 °C to induce the decomposition of the carbonyl compound and the reduction of Pt, forming PtFe or PtCo alloy nanowires.[97] In the synthesis of PtCoFe alloy nanowires, an extra additive 1,2-hexadecanediol was added during the synthesis.[98]

In a recent work, PtIrFe alloy nanowires with face-centred cubic (fcc) lattice were first synthesized *via* the CO procedures, and then the lattice structure was transformed to the more active face-centred tetragonal phase with post-synthetic treatment (Fig. 9). The strong reducing ability of CO enabled the reduction of $Pt(acac)_2$ and $Ir(acac)_2$, and together with Fe that originated from $Fe(CO)_5$, trimetallic nanowires with classic fcc lattice phase and random atomic distribution could be obtained.[100] The presence of the high-melting-point metal Ir was vital to the following thermal treatment and lattice transformations. After being deposited on carbon support and encapsulated by silica shell, the nanowires were subjected to thermal treatment at 690 °C and underwent phase transition without changing in morphology. The obtained PtIrFe nanowires became an ordered alloy with fct phase, and exhibited improved catalytic performances.

CO species normally induce the formation of 2D Pd-based materials, such as nanosheets and nanoplates.[43,101–103] They were considered to bind strongly on the {111} facets of the Pd structures, preventing deposition on the basal surface. Thus, the nanostructures would expand only at the {111} twinning planes, leading to the formation of nanoplates and nanosheets. Recently, there was also work employing CO as ligands for the formation of Pd-based nanowires. PdBi and PdBiM (M = Cu, Co and Mn) nanowires were synthesized in the presence of the carbonyl reagent $Mo(CO)_6$.[104] The complex system contained another two capping agents, tetrabutylammonium bromide (TBAB) and PVP. Also, $Mo(CO)_6$, ascorbic acid and the solvent formamide were all reductive. An orientated attachment mechanism was proposed to indicate that the twisty nanowires were formed *via* the assembly of PdBiCu nanoparticles (Fig. 10). The relatively complex ligand system probably weakened the strong effect of CO on the Pd-based materials. It was found that the presence of the Bi precursor

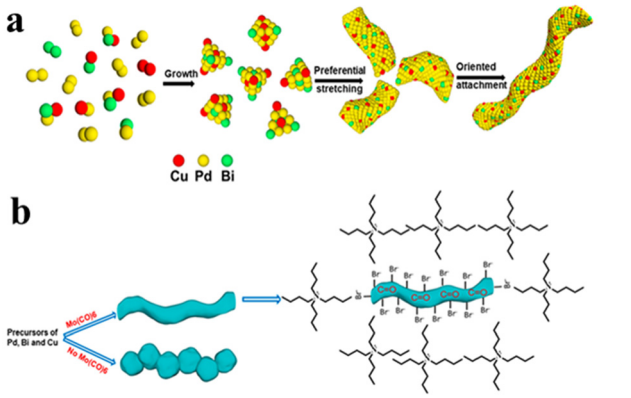

Fig. 10 Schematics illustrating the growth mechanism of PdBiCu nanowires, (a) morphology evolution of nanowires from the precursor nuclei, and (b) effect of $Mo(CO)_6$ presence on the morphology. Reprinted with permission from ref. 104. Copyright 2021 from the American Chemical Society.

was critical for the growth of the 1D nanostructures, while the CO helped the coalescence of the oriented particles.

3.2.3 Organoamine-induced synthesis. Oleylamine has been used in many synthetic routes as the solvent; meanwhile, it was also considered in forming micelle-like structures or linear Au^{+}-oleylamine complexes with Au precursors to induce the formation of ultrathin Au-based nanowires.[105] Pure Au nanowires have been reported to be formed with oleylamine as the ligand, and sometimes as the solvent and reductant at the same time.[106,107] Later, AuAg alloy nanowires were reported by reducing $HAuCl_4$ and $AgNO_3$ in the mixture of oleylamine and oleic acid (Fig. 11a).[108] Other long-chain organoamines are also capable of inducing the growth of Au-based nanowires. Octadecylamine can facilitate the formation of AuCu nanowire coils with glucose as an additional reducing agent,[109] and it was also used in aqueous solution to grow AuAg nanowires with ascorbic acid as the reducing agent (Fig. 11b and c).[110] In terms of forming ultrathin Au-based nanowires, oleylamine is a quite promising reagent, although the formation mechanism has not been completely revealed, and the growth system is not quite versatile enough for morphological adjustments. To date, there have been very few reports on the synthesis of oleylamine-stabilized Au nanowires with thicker diameters.

Recently, there was a report employing oleylamine as the structure-directing reagent to form Pt-based nanowires. The synthesis generated nerve-like PtPb alloy nanowires with various compositions under solvothermal conditions, with toluene as the solvent and borane *tert*-butylamine complex (BTBA) as the reducing agent (Fig. 11d–h).[111] The obtained nanowires did not have well-defined linear or ultrathin morphologies. Their formation was attributed to an oriented attachment process induced by oleylamine, while the metal precursors, the acetylacetonate salts, were also of critical importance for co-reduction and the formation of uniform PtPb grains. The nanowire morphology would cease when the $Pb(acac)_2$ precursor was absent.

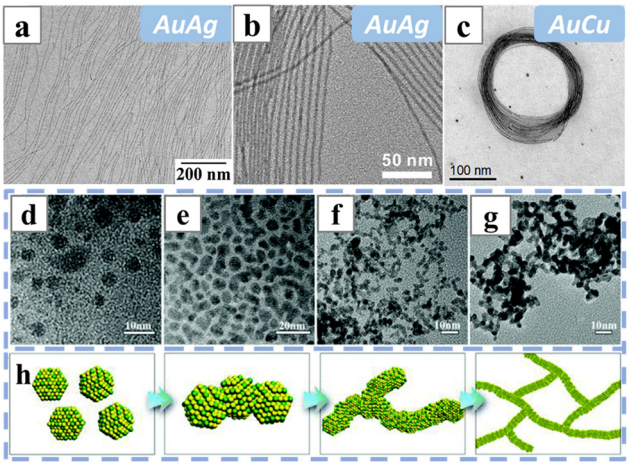

Fig. 11 TEM images of (a) AuAg nanowires synthesized in oleylamine and oleic acid; (b) AuAg nanowires and (c) AuCu nanocoils synthesized with octadecylamine as the structure-directing reagent. (d–g) $Pt_{3.5}Pb$ nanowire intermediates taken at (d) 30 min, (e) 1 h, (f) 2 h and (g) 4 h of reaction times with oleylamine as the structure-directing reagent. (h) Schematics illustrating the formation mechanism of the $Pt_{3.5}Pb$ nanowires, with yellow balls and green balls representing Pt and Pb atoms. Reprinted with permission from ref. 108–111. Copyright 2016 from the American Chemical Society, 2013 from Wiley-VCH GmbH, 2018 from Elsevier.

The *in situ* formed dimethylamine was employed as the structure-directing reagent in a widely applied synthesis of Pt-based nanowires. It was initially developed to synthesize Pt nanowire bundles, and was later extended to a variety of Pt-based alloy nanowires (bundles), including bimetallic PtAu (PtPd),[112,113] PtNi,[114] PtCo,[115,116] PtRu,[117] and ternary PtNiCu[118] and PtNiAu[119] alloy nanowires (Fig. 12). Typically, Pt precursor H_2PtCl_6 and KOH were dissolved in a mixture of ethylene glycol (EG) and *N,N*-dimethylformamide (DMF) and

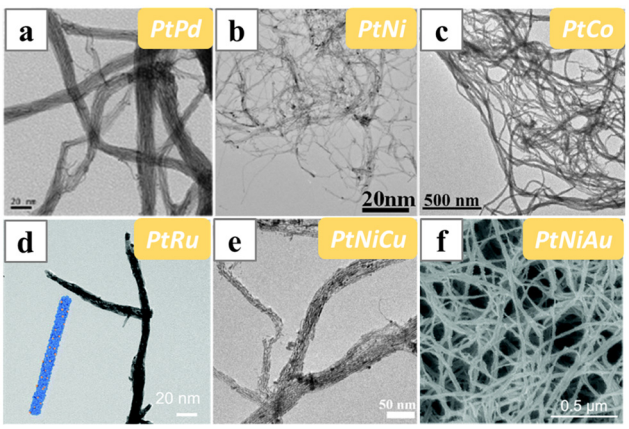

Fig. 12 TEM and SEM images of (a) PtPd, (b) PtNi, (c) PtCo, (d) PtRu, (e) PtNiCu and (f) PtNiAu nanowire bundles synthesized by heating the precursors in the mixed solution of DMF and EG at solvothermal condition. Reprinted with permission from ref. 112, 114, 116–119. Copyright 2019 and 2020 from the American Chemical Society, 2018 and 2021 from Springer Nature, 2020 from the Royal Society of Chemistry.

heated under solvothermal conditions to induce the formation of Pt nanowire bundles. Although the decomposition of DMF released CO, spectroscopic results suggested that there was no CO binding on the nanowire bundles. Therefore, the other decomposition product of DMF, dimethylamine, was deduced to be the structure-directing reagent in this synthesis. In addition, the mechanism study suggested that the Pt nanowire bundles were formed *via* the coalescence of the 1D aligned nanoparticles.[120]

In order to achieve the co-precipitation of the different metals and the formation of alloys, the reaction parameters such as the type and ratio of the metal precursors, the solvent ratio and the amount of KOH, might need further modification, as the co-reduction of metals is sensitive towards the reaction conditions. For instance, strained PtPd nanowires were obtained with $Pt(acac)_2$ and $Pd(acac)_2$ as the metal precursors, and the composition of the alloy could be adjusted by varying the feeding ratio of the metal precursors.[112] PtFe nanowires of various compositions were also obtained with Pt $(acac)_2$ and $Fe(acac)_2$, and by adding oleylamine as the solvent ingradient.[121]

Additional reducing reagent could be introduced into this system to promote the co-precipitation of Pt and metals with low reduction potentials. It was found that the addition of strong reducing agent ascorbic acid was vital for the formation of PtRu alloy nanowires.[117] Without ascorbic acid, only Pt@Ru nanowires with the Ru islands attached to the Pt nanowires were obtained.

In terms of the formation mechanism, the autocatalytic effect was found to play a vital role in forming the alloy structures in this ligand system as well. For instance, Pt and Ni were co-precipitated in the solvothermal condition, yet the reduction system was not capable of reducing Ni^{2+} in the absence of Pt,[114] indicating that Ni^{2+} was reduced *via* an autocatalytic mechanism. It is noted that although the Pt^{4+} was reduced prior to Ni^{2+}, the product obtained was not the core–shell material. Interdiffusion between the two metals led to the formation of Pt_3Ni alloy nanowires. In the same work the authors also believed that the growth of the Pt_3Ni nanowires followed the seed-mediated mechanism, in contrast to the well-accepted oriented attachment mechanism, as no nanoparticle intermediates were observed.

Recently, another amino ligand, 4-aminopyridine, was exploited as a structure-directing reagent for alloy nanowires in aqueous solution. The anisotropic epitaxial growth yielded AuPd alloy nanowires and AuCu alloy nanowire bundles, at different temperature and reaction times (Fig. 13a–d).[122–124] For the synthesis of the AuPd alloy nanowires, nanowires were formed by reducing Au and Pd with ascorbic acid at 80 °C for just 2 min. The nanowire structure cannot form in the absence of either Au, Pd precursors or the 4-aminopyridine. On the other hand, to form AuCu nanowires, the reaction only needed to be reacted at 20 °C for 10 min. Replacing the ascorbic acid with a stronger reducing agent such as $NaBH_4$ compromised the linear structure of the nanowires. Au nanowires could be obtained at this condition with only the Au precursors. Thus,

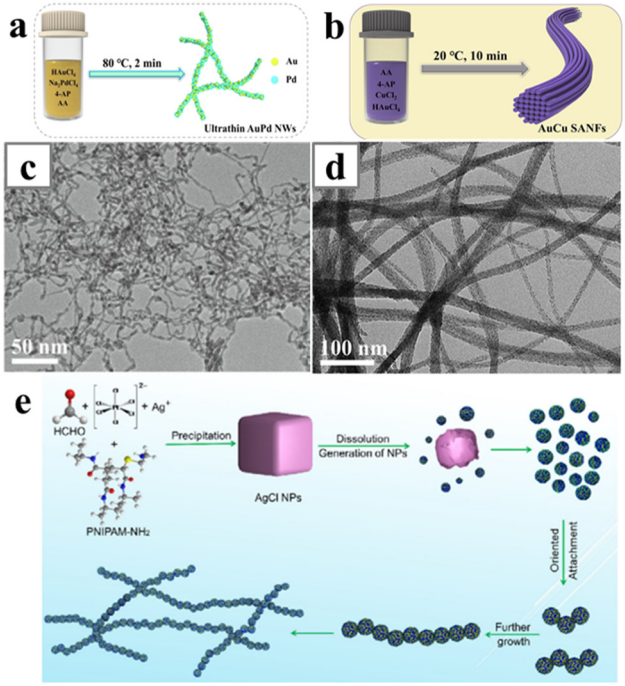

Fig. 13 (a and b) Schematics illustrating the synthetic processes of AuPd nanowires and AuCu nanowire bundles with 4-aminopyridine as the structure-directing reagent. (c and d) TEM image of (c) AuPd nanowires and (d) AuCu nanowire bundles. (e) Schematics illustrating the formation mechanism of the ultrathin AgPt alloy nanowires with PNIPAM-NH_2 as the structure-directing reagent. Reprinted with permission from ref. 122, 123 and 125. Copyright 2022 from Elsevier and 2017 from Springer Nature.

the reaction kinetics is also of critical importance for many ligand systems, and variation of the precursor concentration would cause the change of reduction kinetics. Amine-terminated poly(*N*-isopropylacrylamide) was employed to synthesize wavy AgPt nanowires (Fig. 13e).[125] The amine-terminated polymer was believed to preferentially adsorb onto the {110} and {100} facets of the AgPt nanoparticles, facilitating the oriented attachment of the nanoparticles along the [111] direction.

3.2.4 Non-ionic surfactants as structure-directing reagents. Although the exact mechanisms are not yet fully understood or explained, several non-amphiphilic surfactants have also been employed in the synthesis of metal and metal alloy nanowires, or more exactly chain-like networks. PVP is one of the most widely used surfactants in nanosynthesis. It has been employed in many synthesis studies as a capping agent to stabilize the nanoscale structures against aggregation. In some cases, it was found to induce linear aggregation or formation to form nanowires.

Au-based AuAg[126] and AuAgPd[48] alloy nanowires with ultrathin morphology have been reported synthesized with PVP as the structure-directing ligands in DMF solution (Fig. 14). Both works obtained alloy nanowires with unusual fan-like twisted structures or the Boerdijk–Coxeter–Bernal (BCB) lattice.

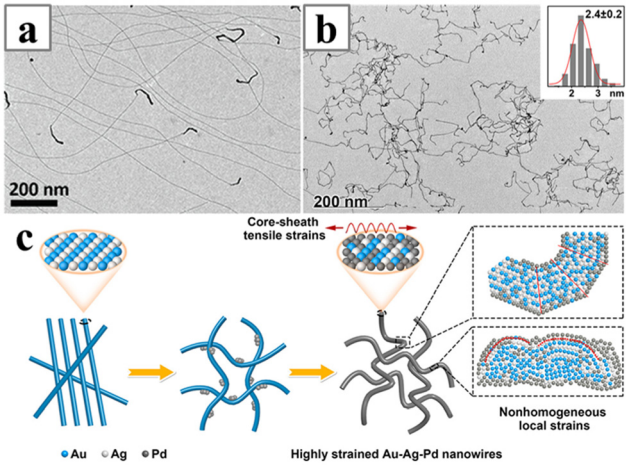

Fig. 14 TEM images of (a) AuAg and (b) AuAgPd nanowires synthesized with PVP as ligand in DMF solution. (c) Schematics illustrating the formation of the highly strained and bent AuAgPd alloy nanowires. Reprinted with permission from ref. 126 and 48. Copyright 2011 and 2021 from the American Chemical Society.

The AuAg alloy nanowires were considered strained, and the nanowire would undergo chiral transformation and twist into double helices upon Pd deposition and the formation of core–shell structures. Similarly, the AuAgPd alloy nanowires were found to be highly strained as well. The mechanism study indicated that during synthesis, single-crystalline AuAg nanowires would first form at the initial stage, followed by the deposition of the Pd sheath, which would cause the lattice structure of the nanowires to transform into fan-like structures.

When PVP was employed as the structure-directing reagent in the syntheses of Pt and Pd-based alloy nanowires, wavy or chain-like networks were usually obtained, suggesting relatively weak control of PVP on the morphology of the nanowires (Fig. 15a–f). For instance, wavy Pt_3Ag nanowires have been formed under solvothermal conditions with PVP as the capping agent.[127] And Pd and PdM (M = Ag, Ni, Cu, Y) nanowire networks have recently been synthesized in a wet-chemical system with DMF and EG as the solvent and reducing agent, and also PVP as the capping agent.[128] PdSn nanowire networks could be formed by employing SnC_2O_4 as the Sn source and adding NH_4Cl as additional capping agent.[129] Alternatively, PdSn nanochains were formed with $(NH_4)_2PdCl_4$ and $SnCl_2$ as precursors, and EG and citric acid as solvent and reductant in solvothermal conditions.[130] PdCu nanowires have also been reported to be obtained with similar reagents in the solvothermal condition.[131] In this case, Cu was believed to be crucial for the formation of the nanowire networks, and in the absence of Cu, only Pd nanoparticles were formed. Alternatively, pure Cu particles with sizes in the hundreds of nanometres were obtained if there was no Pd precursor. Almost all the Pd and Pd-based nanowires synthesized with PVP resemble chain-like networks, and mechanisms involving particle attachment were usually proposed to explain the assembly behaviour of the particles.

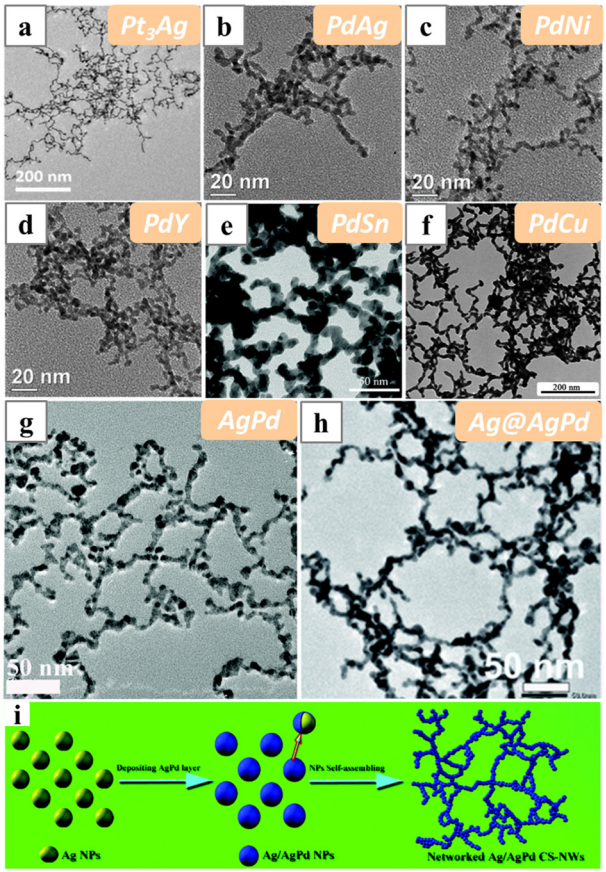

Fig. 15 TEM images of (a) Pt_3Ag, (b) PdAg, (c) PdNi, (d) PdY, (e) PdSn, (f) PdCu, (g) AgPd and (h) Ag@AgPd nanowires synthesized with PVP as the structure-directing reagent in aqueous solutions. (i) Schematics illustrating the oriented attachment of Ag@AgPd nanoparticles into networked Ag@AgPd nanowires. Reprinted with permission from ref. 127–129, 131, 133 and 134. Copyright 2020 from Springer Nature, 2018 and 2021 from the Royal Society of Chemistry, 2017 from Elsevier.

There was also an unusual PVP-involved synthesis. Ru–Pd (Rh and Ag) alloy nanowires were generated by first synthesizing Ru nanoparticles with diameters of 2–3 nm with a polyol process, and then reducing the second metal together with the Ru nanoparticles in the presence of PVP under a solvothermal condition.[132] The formation of the nanowire structure was attributed to an attachment process assisted by the heterogeneous nucleation of Pd, and the linear structure was obtained as a balance between the van der Waal's interaction and electrostatic repulsion between the particles. PVP in this work was believed to function as a stabilizer to assist the attachment process.

The PVP derivative polyvinylpyrrolidone imine was employed to induce the formation of AgPd nanowires in polyol solutions (Fig. 15g). Again an assembly mechanism was proposed: the two metals were first reduced into AgPd nanoparticles and then assembled into nanowire networks.[133] And interestingly, Ag@AgPd core–shell nanowires could also be obtained by the assembly of Ag@AgPd core–shell nanoparticles (Fig. 15h and i).[134]

Sometimes, additional reagents need to be introduced in order to assist the co-reduction of metals during one-pot synthesis. With the presence of sulphite (SO_3^{2-}) and proton (H^+), twisty PdNi nanowires can be synthesized in PVP-containing aqueous solution under hydrothermal conditions.[135] The effect of sulphite was found to be crucial for the co-precipitation process, and pure Pd nanowires could be obtained with it. H^+ was found necessary for the formation of 1D morphology: increasing the pH would lead to the emergence of nanoparticles. While the HCl that was used to dissolve $PdCl_2$ was considered as the proton source, supplying extra protons with H_2SO_4 can also lead to the formation of twisty nanowires, and it is noted that HCOOH was also involved in the system. A similar synthesis was developed to grow the ternary PtCuNi nanowires, with the solvent water replaced by EG.[136] Sulphite also served as the key reagent for this electroless-plating process that enabled the co-precipitation of the metals, especially the reduction of Ni^{2+}. Hence, sulphite is one useful reagent that helps the co-reduction and precipitation of metals, and induces alloy formation in the solution-based synthesis of alloy nanowires.

Additionally, there have also been reports about using other commercial surfactants, such as NP-40 and Pluronic F127, to synthesize Pd-based nanowires. Nanowires formed with these reagents had morphologies similar to those formed with PVP. Reducing K_2PtCl_4 and K_2PdCl_4 with ascorbic acid in the presence of F127 under hydrothermal conditions can yield PdPt nanowires.[137] Introducing H_3BO_3/DMAB as the B source and NaH_2PO_3 as the P source during the synthesis can lead to the formation of PdBP nanowires.[138] Chain-like PdBi and PdBiAu structures can be synthesized *via* a hydrothermal method, with DMF and oleylamine as the solvent and F127 as the additive.[139] Alternatively, NP-40 as the structure-directing agent can be used to produce PdCu as well as PdFePb (and PdPb or PdFe) alloy nanowires.[140,141] Both reports employ the borohydride reducing system, with either $NaBH_4$ or KBH_4 as the reducing agent in ice-cold aqueous solution. Formation of the nanowire structure was believed to be an anisotropic epitaxial growth guided by NP-40.

Apart from the abovementioned families of ligands, there are also syntheses of alloy nanowires or chain-like structures employing uncommon ligands or even without molecular ligands. For instance, using *N,N*-dimethylacetamide as the solvent and formamide as the ligand, binary PtCu, PtCo and ternary PtCuCo nanochains could be synthesized in solvothermal conditions.[142]

Overall, solution-based methods can be highly diverse in terms of the metal precursors, structure-directing reagent, reduction systems and the reaction conditions. Single or combinations of molecular and polymeric morphological directing agents or ligands are necessary during the reduction and deposition of metal to induce 1D growth. The most widely used ligands are CTAC (or CTAB), CO, various amine species and polymeric surfactants such as PVP. Micelle-templates or oriented attachment are the commonly proposed mechanisms in the solution-based synthesis. It is clear that the solvent and the reduction system need to be carefully matched with the ligand to enable the anisotropic growth of metal crystals.

3.3 Other methods

Besides the abovementioned template-based or solution chemical syntheses, several uncommon methods have also been developed to obtain alloy nanowires, and each method is specific to a certain type of alloy nanowire.

3.3.1 Spinodal decomposition and dealloying. Recently, a dealloying strategy was developed to synthesize Al-based high-entropy alloy nanowires.[143] Typically, Ni, Co, and Ru were first melted to form a solid solution, followed by the introduction of a fourth metal (either Mo, Cu, V or Fe). The solid solution was then melted in Al to form an Al-based alloy. Interestingly, the metals would undergo spinodal decomposition and exist as thin nanowires. High-entropy Al–Ni–Co–Ru–X alloy nanowires were then obtained after etching of the pure Al phase with alkaline solution. During the dealloying procedure, a layer of spinel oxide also formed on the surface of the alloy nanowire.

3.3.2 Template-less electrodeposition. Screw-like single-crystalline PtPd nanowires with diameters around 30 nm have been prepared with a template-less electrodeposition method on clear glass-carbon electrodes (Fig. 16).[144] The formation of the nanowires was achieved by first imposing a relatively negative reduction potential to initiate nucleation, and then applying a square-wave potential of 100 Hz frequency to maintain the growth of the nanowires. The molar ratio of Pd^{2+} and Pt^{4+} in the electrolyte solution was 4 : 1, and deviation from that ratio would lead to failure of the formation of the PdPt nanowires: no nanowires could be obtained with pure K_2PtCl_4 or H_2PdCl_2 as the precursor. And the composition of the final PdPt nanowires was not controlled by the feeding ratio of the precursors, but rather by the upper potential limit of the square-wave potential applied during growth.

3.3.3 Direct-current arc-discharge. A direct-current arc-discharge process was developed to generate Ni–Co chain-like nanowires.[145] The high-temperature arc process evaporated the anode containing both Ni and Co into a homogeneous atomic mixture. The atomic mixture then crystallized to form chain-like Ni–Co particles and aggregated to a web-like product at the top of the discharge chamber. The compositions of the

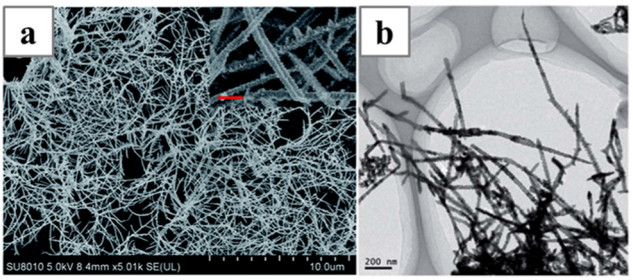

Fig. 16 (a) SEM and (b) TEM image of the PdPt nanowires synthesized with template-less electrodeposition. Reprinted with permission from ref. 144. Copyright 2018 from the Royal Society of Chemistry.

alloy could be adjusted by the metal ratio in the anode. This method employed neither ligand nor solvent, and it could also produce pure metal nanochains. The obtained alloy chains have diameters of 40–50 nm and length up to several micrometres. Surface oxidation would occur immediately after in nanochains exposed to air, generating core–shell structures.

4. Forming alloy on existing nanowires

Compared with the direct formation approaches, synthesizing alloy nanowires based on existing nanowire structures circumvents the challenge of inducing 1D growth in metallic crystals. In cases of forming ternary or more alloys, the ingredients of the alloys can be introduced simultaneously or sequentially. Depending on the reactivity of the templating nanowires and the metal precursors, either replacement reactions, heterogeneous doping or heterogeneous nucleation would occur when the templating nanowires were mixed with the metal precursors (Fig. 17). The heterogeneous doping process was guided by the spontaneous interdiffusion between the metals, and a thermal annealing process could be employed to mix the metals in the core and shell layers if a core–shell structure was initially obtained.

4.1 Forming alloy shell on metal nanowires

Synthesis of the core–shell nanowires with shell made of the alloy of the core metal can often be achieved simply with one-pot procedures. Due to the difference in the reduction potential, the second metal only starts to be reduced after the reduction and formation of the core nanowire, even if all the metal precursors are added together at the beginning of the reduction process. For instance, Au@PtAu nanowires could be obtained based on an α-naphthol-induced synthesis of Au nanowires (Fig. 18a).[146] Pt was only present in the shell layer

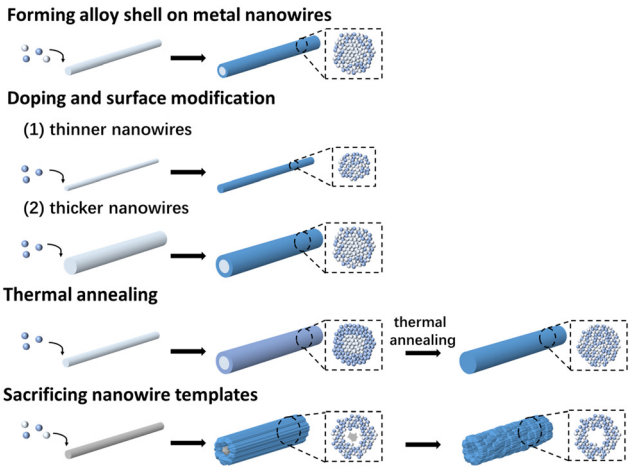

Fig. 17 Schematics showing the different scenarios of forming alloy (core–shell) nanowires from existing 1D nanostructures.

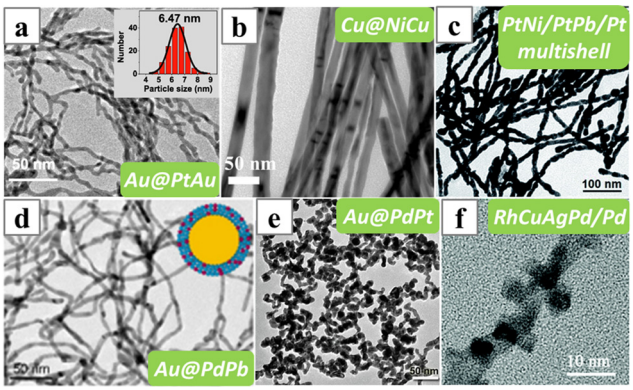

Fig. 18 TEM images of (a) Au@PtAu, (b) Cu@NiCu, (c) PtNi/PtPb/Pt, (d) Au@PdPb, (e) Au@PdPt core–shell or multishell nanowires and (f) RhCuAgPd/Pd nanowires synthesized depositing the alloy shell on the preformed metal nanowires. Reprinted with permission from ref. 146–151. Copyright 2021 from Science Press and Elsevier, 2017 from the Royal Society of Chemistry, 2020 from Springer Nature, 2017 from the American Chemical Society.

as its reduction only started after the formation of the core Au nanowires.

Besides, reaction temperature can be used to trigger the formation of the alloy shell. Cu@NiCu core–shell nanowire can be formed with a method derived from the synthesis of the Cu nanowires (Fig. 18b).[147] Although both the $Cu(acac)_2$ and $NiCl_2$ were added at the beginning of the synthesis, the Ni only exists in the surface alloy layer as its reduction only occurred after the temperature was raised from 185 °C to 220 °C.

Nevertheless, a multi-step procedure is also quite plausible for the synthesis of core–shell alloy nanowires. PtNi/PtPb/Pt multishell nanowires were obtained by first synthesizing the PtNi nanowires in oleylamine solvent with CTAB as the structure-directing reagent, and then the reaction mixture was cooled slightly followed by the addition of $Pb(acac)_2$ to induce the formation of the PtPb shell (Fig. 18c).[148]

Less commonly, alloy shells can be deposited on nanowires made of a foreign metal. The core and the shell materials must be carefully considered to allow the epitaxial growth of the shell on the core nanowires. PdPb (or Pd) shell can grow epitaxially on Au nanowires to form Au@PdPb nanowires, due to the small lattice mismatch between Au and Pd (Fig. 18d).[149] Also, networks of Au@PdPt core–shell nanowires were synthesized by first reducing the $HAuCl_4$ with sodium citrate to form *in situ* Au nanowires, and then adding the Na_2PdCl_4 and K_2PtCl_6 sequentially, and lastly another reducing agent ascorbic acid (Fig. 18e).[150] Interestingly, the residue Au ions must be kept low during the reduction of Pd and Pt, as the ternary alloy Au–Pd–Pt would have a larger lattice mismatch with the Au nanowires, which would lead to the formation of isolated nanoparticles instead of coaxial nanowires.

When the interfacial energy between the alloy materials and the seed nanowires is too high to form uniform core–shell structures, nanowires with surface alloy islands are obtained. RhCuAgPd/Pd nanowires were synthesized with Pd nanowires

as the seeds (Fig. 18f).[151] The metal precursors were added after the formation of the Pt nanowires, and were reduced by the residual ascorbic acid left in the reaction mixture during the formation of the Pd nanowires.

4.2 Doping and surface modification

Post-synthetic doping and surface modification generate alloy nanowires based on the interdiffusion of metals, an entropy-driven process that occurs when atoms of different metals are brought together. Also, the diffusion kinetics of the metals must be sufficient to allow the spontaneous dispersion of the second metal into the lattice of the original nanowire and form solid solutions after being deposited onto the existing nanowires. For ultrathin nanowires, the interdiffusion process usually occurs easily; and in some cases, the formation of the alloy would even cause change in the lattice structure, inducing strain in the lattice and change in the morphologies of the nanowires. If the core nanowires were too thick to achieve homogeneous mixing of the different metals, core–shell nanowires with an alloy shell would be obtained.

Strictly speaking, many of the abovementioned direct syntheses of Pt-based alloy nanowires also followed the heterogeneous doping mechanism. Although all metal precursors were added simultaneously during the one-pot syntheses, Pt with the highest reduction potential would be reduced first and form nanowires with the assistance of the structure-directing reagent, and the second metal was then deposited on the Pt nanowires to form the alloy nanowires. Alternatively, heterogeneous doping could also be carried out as a separated step, with the second metal being reduced in a different environment. In a recent work, $Ga(acac)_2$ was reduced with ascorbic acid in the presence of preformed Pt nanowires to form ultrathin PtGa nanowires (Fig. 19a–d).[152] A more obvious procedure was the formation of PtSn nanowires on carbon support.[153] Pt precursors were first mixed with the carbon support and reduced by HCOOH for different times to obtain nanowires, followed by the addition and reduction of $SnCl_2$ with HCOOH for 48 h to form the alloy nanowires.

In a recent work, the early transition metal W was introduced into the pre-formed Pt nanowire through an electrochemical etching process to form PtW alloy nanowires.[154] An amorphous WO_x shell was first grown onto the Pt nanowires by depositing W precursors at 300 °C, followed by etching of the oxide layer and doping of W in the nanowires. Similar to other alloys, the reduction of W was attributed to the autocatalytic effect on the Pt surface, where the surface Pt–H acts as a strong reducing agent to reduce W. After that, the interdiffusion between the W and Pt in this electrochemical environment would allow the formation of the PtW nanowires.

Oleylamine-stabilized ultrathin Au nanowires have been employed as precursors for Au-based alloy nanowires. AuM (M = Pt, Cu and Pd) was obtained *via* heterogeneous doping processes occurring at the liquid–liquid interface of EG and hexane (Fig. 19e–i).[155] The as-synthesized Au nanowires were first dissolved in the non-polar phase, while the metal precursors were in the polar phases and brought to the interface by

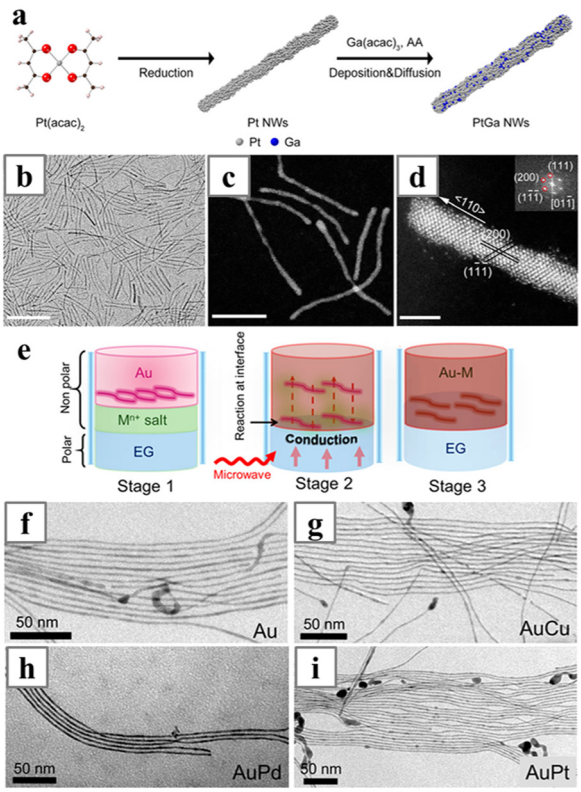

Fig. 19 (a) Schematics illustrating the two-step synthesis of PtGa nanowires. (b) TEM, (c) HAADF-STEM and (d) atomic-resolution aberration-corrected HAADF-STEM image (with the corresponding FFT pattern) of the PtGa nanowires. (e) Schematics illustrating the formation of Au–M nanowires at the liquid–liquid interface. (f–i) The resulting TEM images of (f) Au, (g) AuCu, (h) AuPd, and (i) AuPt nanowire arrays. Reprinted with permission from ref. 152 and 155. Copyright 2019 and 2018 from the American Chemical Society.

the oleic acid additive. Glucose was employed as the reducing agent, and the reduction was carried out with microwave heating.

Alternatively, double helical AuAg and AuPd nanowires/nanoropes have been shown to be formed by directly reducing Ag or Pd in the presence of oleylamine-stabilized ultrathin Au nanowires (Fig. 20).[156,157] The double helical AuAg nanowires were formed in the non-polar phase while the AuPd nanoropes were synthesized in aqueous solution. Either way, the interdiffusion of the metals can occur at room temperature and simultaneously with reduction of the second metal. The ultrathin Au nanowires were believed to be single crystalline and elongating along the [111] direction of the fcc lattice, and the alloying process altered the lattice structures of the ultrathin nanowires. The resulting lattice structures contained a lot of fan-like segments. While the BCB lattices should be straight in outline, the disordered lattice structure in the double helical nanowires may be the complex intermediates which were kinetically trapped half-way in between the transformation from fcc lattice to BCB lattices. The alloying process also imposed strain in the nanowires and twisted the straight nanowires into

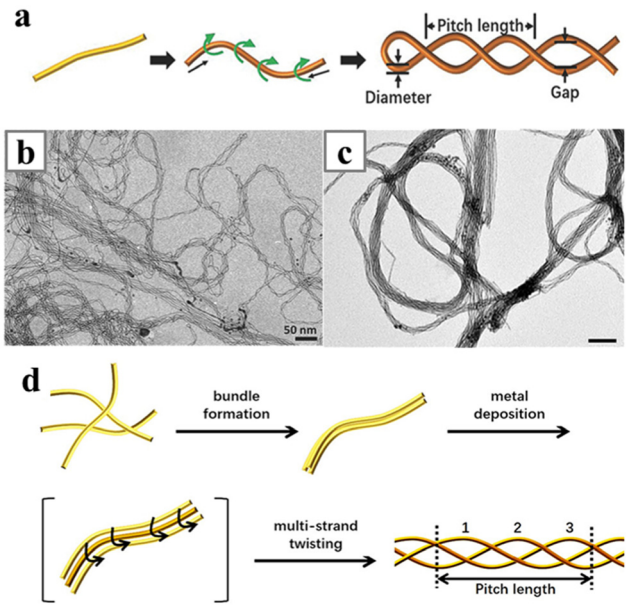

Fig. 20 (a) Schematics illustrating the twisting of Au–Ag double helix nanowires. (b) TEM image of ultrathin Au–Ag alloy helices. (c) TEM image of AuPd nanoropes. (d) Schematics illustrating the braiding of AuPd nanoropes. Reprinted with permission from ref. 156 and 157. Copyright 2018 from WILEY-VCH GmbH and 2020 from the American Chemical Society.

double helices. The strain and the lattice structure in the double helical alloy nanowires can be further adjusted with a H_2O_2-assisted fusion process, producing solid AuPd nanowires with optimized internal strain for catalytic applications.[158]

In contrast, surface deposition would not have a significant effect on the morphologies of nanowires with large diameters, but would form an alloy surface layer that greatly changes the physical and chemical properties of 1D nanostructures. Ag nanowires (or nanotubes) with improved chemical stability and mechanical strength can be obtained with surface-doping of Pd *via* galvanic replacement in the presence of the reducing agent ascorbic acid.[159] The morphology and composition of the final structure can be adjusted by pH, which directly affects the reducing ability of ascorbic acid. Similarly, an Ir layer can be formed on the Ag nanowire surface and form Ag@AgIr core–shell nanowires with a two-step heating procedure.[160] The Ag core could then be etched with HNO_3 to yield the AgIr alloy nanotubes.

4.3 Thermal annealing

Thermal annealing is one conventional method to produce alloy materials.[37,161] However, applying thermal annealing in the synthesis of alloy nanowires can be quite challenging. The nanowires, especially those that are ultrathin in nature, might not be able to maintain 1D morphology at elevated temperatures, as surface diffusion and atom migration would inevitably happen in company with the interdiffusion process. On the other hand, spontaneous interdiffusion of metal atoms would occur in ultrathin nanowires at room temperature, generating alloy nanowires directly during synthesis or *via* the post-synthetic deposition process. Thus, thermal annealing can only be applied to the thick core–shell 1D nanostructures to generate alloys with ordered crystalline phase.

One typical demonstration of this approach was the synthesis of Cu_3Au alloy nanowires with precise composition *via* the thermal annealing of the core–shell Cu@Au nanowires (Fig. 21).[162] The annealing process was performed under the forming gas atmosphere so as to suppress the wire sintering during the high-temperature process. The Cu–Au forms a series of solid solutions at different annealing temperatures, and intermediate CuAu alloy nanowires with $L1_0$ phase were obtained when the temperature was below 200 °C. The $L1_2$ Cu_3Au phase would emerge above 220 °C, and complete conversion to the uniform Cu_3Au $L1_2$ phase was realized at 320 °C. Since the alloy process occurs by the interdiffusion of the core and shell materials, both raising the temperature and lengthening the annealing time would favour the formation of the alloy Cu_3Au $L1_2$ phase. Compared with the pristine Cu nanowires and the Cu@Au core–shell nanowires, the final Cu_3Au alloy nanowires exhibit improved thermal stability. When annealed in air, the Cu_3Au only undergoes phase transition and morphology change above 250 °C, whereas phase transition in the other two nanowires starts at only 150 °C (Cu) and 200 °C (Cu@Au).

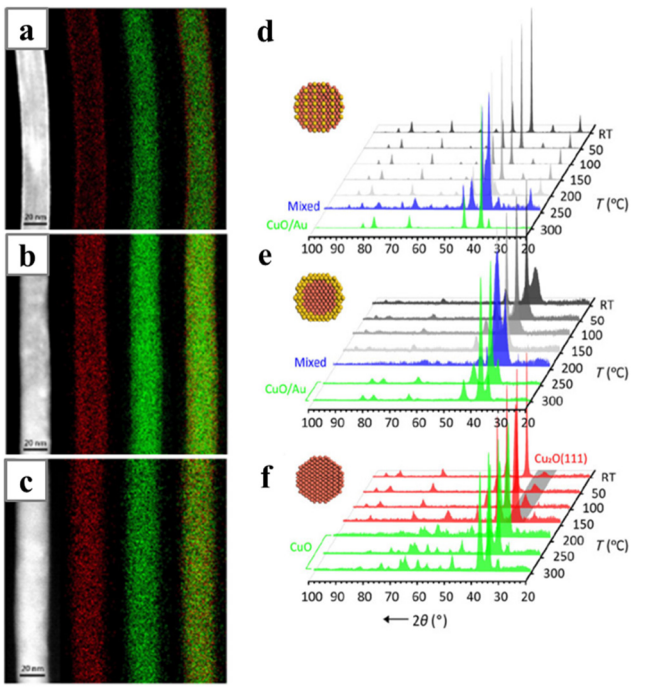

Fig. 21 (a–c) HAADF-STEM images and EDS elemental mappings of (a) pristine Cu@Au core–shell nanowire (b) an intermediate obtained after annealing the Cu@Au nanowires at 200 °C and (c) CuAu alloy nanowires obtained after annealing the Cu@Au nanowires at 320 °C. XRD patterns of (d) Cu_3Au, (e) Cu@Au core–shell prepared at 140 °C and (f) Cu nanowires after annealing in air for 1 hour at elevated temperatures. Reprinted with permission from ref. 162. Copyright 2020 from Springer Nature.

4.4 Sacrificing nanowire templates

When nanowires of the more active metal were employed as template to synthesize alloy nanowires, the alloying process would happen simultaneously with the galvanic replacement process. Sometimes, extra reducing agents were added to prevent overreaction between the metal nanowires and salt precursors. Often, tubular and porous structures with alloy shells were obtained, as the reduction and deposition always start from the surface of the template nanowires.

PdCu–SnO_2 nanowires could be formed by direct galvanic replacement between Na_2PdCl_4 and the Cu–SnO_2 nanowires,[163] while the porous PdAg nanowires need the presence of ascorbic acid in the galvanic replacement process between the Ag nanowires and Pd precursors at 80 °C.[164] An opposite case is the formation of PtCu nanowires *via* the post-synthetic alloying of Cu nanowires. The Cu nanowires can directly react with H_2PtCl_4. However, in the absence of the reducing agent ascorbic acid, only surface-decorated Pt nanoparticles were obtained.[165] In another work, the formation of either solid PdCu nanowires or hollow PdCu nanotubes was determined by a ligand, dimethyl distearylammonium chloride,[166] which was believed to adsorb strongly on the (100) facets of the Cu nanowires (Fig. 22). In the presence of the ligand, the galvanic replacement could only occur at the ends of the Cu nanowires, leading to the formation of the tubular structure (Fig. 22d and e).

Te nanowires have been employed as a hard nanoscale template for the synthesis of various metal and metal alloy nanowires, such as Pd, PdPt and PdAu nanowires (Fig. 23a–e).[167,168] The Te nanowires were oxidized with metal salt precursors. Therefore, the formation of the nanowires was achieved by galvanic replacement between the metals and the sacrificing Te template. Additionally, the sequence of adding metal precursors is crucial for the composition of the alloy nanowires. For instance, in order to form the quaternary PtPdRuTe alloy,[169] the $RuCl_3$ needed to be mixed first with the Te nanowires to initiate the galvanic replacement and yield the $RuTe_2$ nanowire, followed by the addition of the Pt and Pd precursors. If all the metal precursors were added together, only ternary PtPdTe nanowires could form, as Pt and Pd possess high reduction potential, and they would deposit on the surface of Te nanowire first, inhibiting the galvanic replacement reaction between Te and Ru^{3+}. Similarly, PtAgTe and PtRuAgTe nanowires could be obtained at solvothermal condition, with the stepwise transformation from Te nanowires to $AgTe_2$ nanowires and finally the PGM-containing alloy nanowires.[170] This templating method also offered a simple route to produce porous alloy nanowires, such as AuPt and PdPt porous nanowires. Typically, the Te-containing alloy nanowires were firstly formed *via* galvanic replacement between the Te nanowires and the metal precursors, and the residue Te in the alloy nanowires was then etched with NaClO to produce the porous morphology (Fig. 23f and g).[171,172]

Metal ions and polymeric fibres, including biological macromolecules that form linear assemblies in solution and electrospun nanofibers,[173,174] could assemble into 1D nanostructures and act as self-sacrificing templates to synthesize 1D alloy nanowires.[175–179] For instance, insulin amyloid fibrils (INSAFs) have been exploited to synthesize PtRh[180] and

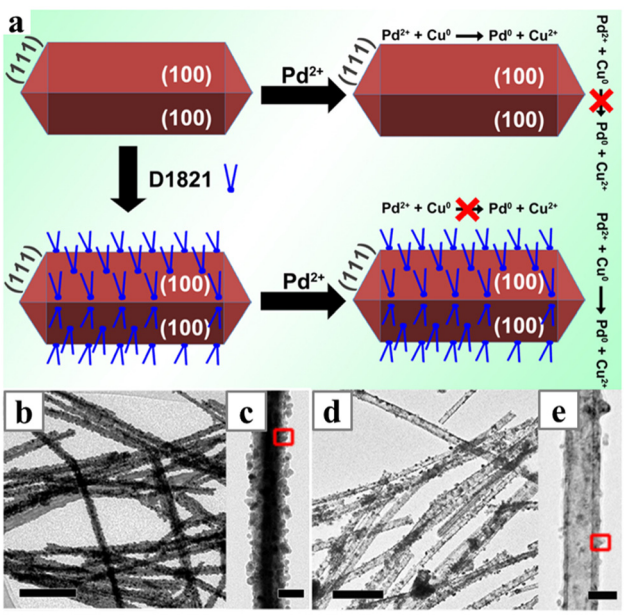

Fig. 22 (a) Schematics illustrating the selective galvanic displacement reaction on different facet of Cu nanowires; and the resulting TEM images of PdCu (b and c) nanowires and (d and e) nanotubes. Reprinted with permission from ref. 166. Copyright 2020 from Elsevier.

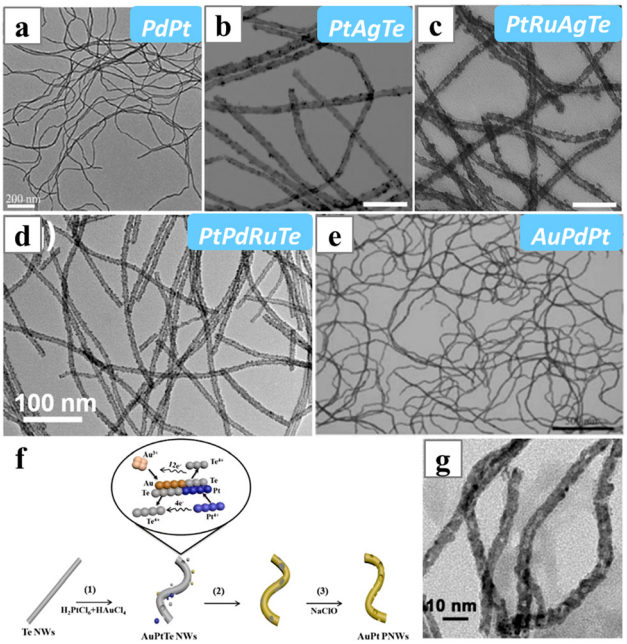

Fig. 23 TEM images of (a) PdPt, (b) PtAgTe, (c) PtRuAgTe, (d) PtPdRuTe and (e) AuPdPt nanowiress synthesized *via* replacing the Te nanowires with metal precursors. (f) Schematics illustrating the formation mechanism of AuPt porous nanowires and (g) the resulting TEM image of AuPt porous nanowires. Reprinted with permission from ref. 167, 169–171. Copyright 2019 from the Royal Society of Chemistry, copyright 2017, 2019 and 2022 from the American Chemical Society.

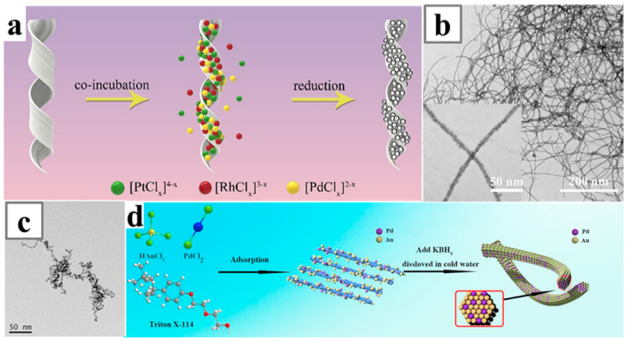

Fig. 24 (a) Schematics illustrating the formation of PtRhPd nanocoils and (b) TEM image of the PtRhPd nanocoils. (c) TEM image of AuPd nanowires synthesized with Triton X-114 as the structure-directing reagent and (d) the schematics illustrating the formation mechanism of the Triton X-114 induced synthesis. Reprinted with permission from ref. 181 and 182. Copyright 2020 from the American Chemical Society and 2020 from Elsevier.

PtRhPd[181] nanowires (Fig. 24a and b). The mixture of the metal precursors was first adsorbed onto the bio-templates, and then reduced with the strong reducing agent $NaBH_4$ to yield alloy nanowires, or more specifically, nanochains made of small alloy nanoparticles. Afterwards, the biological template INSAF could be removed by washing with ammonia.

Sometimes, co-assembly of metal ions with organic surfactants could form insoluble fabric nanostructures and act as self-templates for the formation of metal nanowires; for instance, incubating $HAuCl_4$ and $PdCl_2$ with the commercial surfactant Triton X-114 to form fabric assemblies (Fig. 24c and d).[182] Reducing the intermediates with KBH_4 yielded AuPd ultrathin nanowires. Similar procedures have also been employed to produce PdCu alloy nanowires.[183]

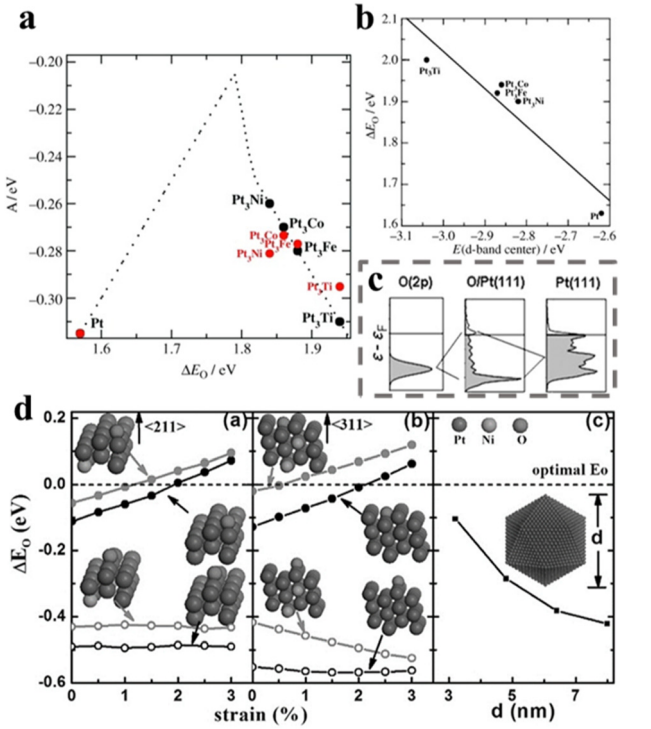

Fig. 25 (a) Model of the activity (*A*) at a cell potential of 0.9 V as a function of the adsorption energy of oxygen, ΔE_O. The predictions of the model for Pt_3M (M = Ni, Co, Fe, Ti) alloys are shown relative to the predictions for Pt at the DFT-calculated values of ΔE_O. (b) The correlation between the d-band center and ΔE_O (c) sp-broadened 2p orbital for O(g), projected p density of states of oxygen atoms on Pt(111), and projected d density of states of Pt(111). (d) DFT calculations of oxygen adsorption energy. ΔE_O as a function of compressive strain on (d(a)) (211) and (d(b)) (311) surfaces. The filled circles represent ΔE_O values on the hollow sites while the open circles represent the bridge sites. The black and grey curves correspond to ΔE_O values on pure Pt and Pt_3Ni surface with top-layer Ni atoms completely removed. (d(c)) ΔE_O on the (111) facet of the Pt nanoparticles as a function of the particle size. Reprinted with permission from ref. 36 and 39. Copyright 2006 and 2015 from Wiley-VCH GmbH.

5. Metal alloy nanowires as electrocatalysts

Like the pure metal nanowires, most of the noble metal-based alloy nanowires are excellent electrocatalysts, as normally at least one of the nanowire compositions is an active catalyst for one or more electrochemical reactions.

5.1 Oxygen reduction reactions

The oxygen reduction reaction (ORR) is the key process that happens at the cathode of fuel cells. Its slow kinetics remains the most challenging problem for the fuel cell industry.[184] To date, platinum (Pt) remains the most promising and applicable commercial ORR catalyst, and replacing the benchmark Pt/C with Pt-based alloy nanowires with superior activity and stability is one meaningful way to reduce the usage of this expensive noble metal.[185] Moreover, forming PtM alloys with non-noble metals can further cut the cost of the catalysts.

While Pt is considered the most reliable metal catalyst for oxygen reduction, the binding energies of the oxygen species are still too strong on the Pt surface (typically the (111) facets) according to the volcano plot and calculations (Fig. 25a–c).[36] Formation of PtM alloy is believed to decrease the binding energies of O_2 and oxygen species (ΔE_O) on the Pt surface, leading to enhancement of the ORR activities. Conventionally, the d-band centre, which is the average energy of d states that bind to the oxygen on the catalyst surface, is often evaluated as it is a direct indication of the ΔE_O. A decrease in the d-band centre would lead to a less-filled d-band and thus weaker binding towards the surface oxide. Incorporating another transition metal, such as Ni and Co, would cause shrinkage of the skin Pt–Pt distance (the strain effect) as well as transfer of charge from Pt to the doping metal *via* the d-d interaction (the ligand effect), decrease of the d-band centre of the Pt and enhancement of the ORR activities (Fig. 25d).[39] Based on this prediction, various PtNi, PtCo, PtFe, PtSn, PtCu, and PtPb alloy nanowires have been developed and demonstrated as superior ORR catalysts.

Besides Pt, Pd alloy is also an emerging material for ORR, owing to the similar physical and chemical properties of Pt and Pd. Many Pd-based alloy nanowires have also been applied as ORR catalysts, such as PdAu, PdNi, PdCu and PdBi nanowires. Similar to Pt, formation of PdM alloy also offers the ligand and strain effect on the electronic structure of Pd, lowing the d-band centre of Pd and offering much improved performances.

While the PtNi alloy has a more optimized electronic structure than the pristine Pt, a NH_3 treatment was developed recently to further fine-tune the ΔE_O on the PtNi nanowire surface.[67] The as-synthesized PtNi nanowires were first washed with acetic acid to obtain a Pt-rich skin, followed by the NH_3 treatment. NH_3 has a slightly stronger adsorption to Ni than Pt, and this would promote the spillover of Ni and increase the Ni composition at the surface, decreasing the d-band centre and ΔE_O (Fig. 26).[67] The PtNi-C/NH_3 nanowires exhibited specific (SA) and mass activities (MA) of 3.86 mA cm^{-2} and 1.02 A mg_{Pt}^{-1} respectively, much better than the benchmark Pt/C and the untreated PtNi/C nanowires.

On the other hand, the strain effect of alloying was also recently shown to be quite sensitive to the alloy compositions.[112] A series of strain-modulated PtPd nanowires was synthesized *via* the solvothermal process in the mixed solvent of DMF and EG. The nanowires have the BCB lattice with

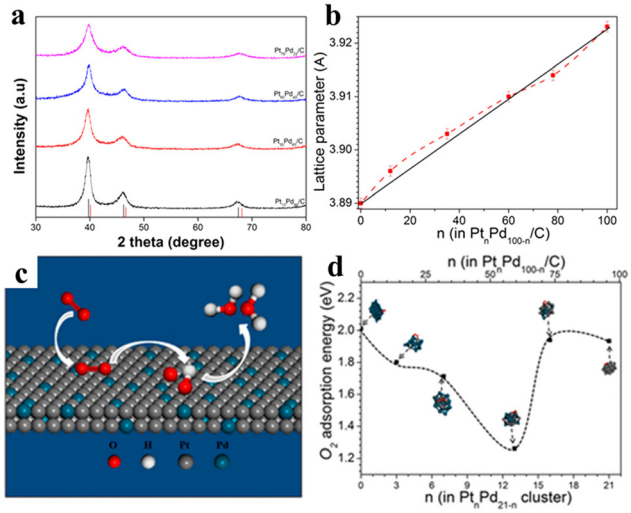

Fig. 27 (a) XRD patterns of $Pt_{12}Pd_{88}$/C, $Pt_{35}Pd_{65}$/C, $Pt_{60}Pd_{40}$/C, and $Pt_{78}Pd_{22}$/C nanowires (b) lattice parameters for Pt_nPd_{100-n} NWs/C on the relative composition of Pt%, the solid black line is according to Vegard's law based on the lattice parameters of Pt and Pd. (c) Schematic illustration of the catalytic synergy for the ORR over PtPd nanowires featuring the (111) facet. (d) Adsorption energy for molecularly adsorbed O on Pt_nPd_{21-n} clusters (n = 1–21) obtained by DFT calculations. Reprinted with permission from ref. 112. Copyright 2020 from the American Chemical Society.

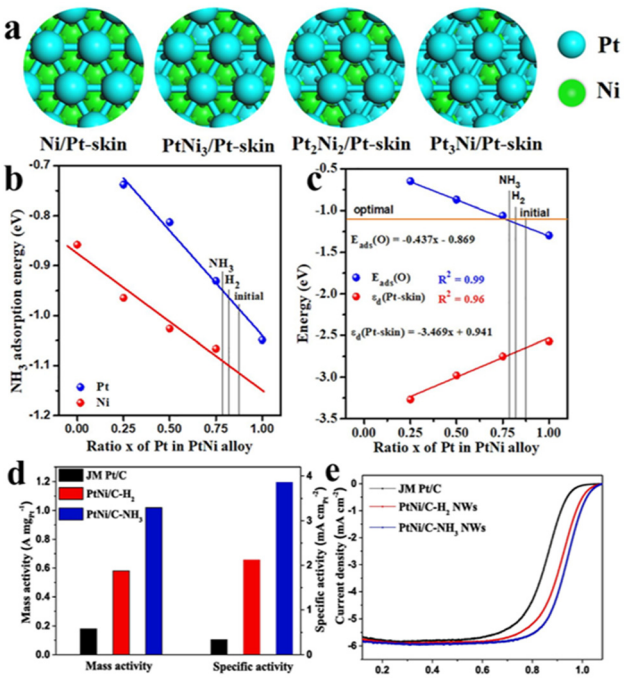

Fig. 26 (a) Models of Pt-skin covered PtNi alloys with different Pt : Ni ratio. (b) NH_3 adsorption on Pt or Ni atoms of PtNi alloy with different Pt : Ni ratio. (c) d-band center (ε_d, red line) of Pt-skin covered on PtNi alloy with different Pt : Ni ratio and corresponding O adsorption energy (blue line). (d) mass and specific activities of Pt/C, PtNi/C–H_2 NWs and PtNi/C–NH_3 NWs at 0.9 V (*vs.* RHE). (e) ORR Polarization curves of PtNi/C–H_2 NWs, PtNi/C–NH_3 NWs and Pt/C. Reprinted with permission from ref. 67. Copyright 2021 from Elsevier.

mostly (111) facets, which are favourable for ORR. Moreover, XRD characterizations indicated that the alloying process caused either shrinkage or expansion of the lattice in the nanowires (Fig. 27). Lattice shrinking would lead to compressive Pt–Pt distance and weakening of the adsorption energy of oxygen species (*OH and *O) on the nanowire surface. The DFT calculation indicated that nanoclusters with 75%Pt in the alloy can bind more O_2 species and less OH and O. Thus, the nanowires with the optimized composition of $Pt_{78}Pd_{22}$ had a subtle shrinking in lattice and exhibited the best catalytic activity among the series.

Although the d-block transition metals are usually used for alloying with Pt and Pd, main group metals such as Ga can also be incorporated into Pt to form alloy nanowires with improved ORR performance.[152] Instead of the d–d interaction, the Ga varied the electronic structure of Pt *via* the p–d hybridization interaction, causing redistribution of electron density on the skin Pt(111) surface and the downshift of the d band centre. This led to the boosting of ORR activities. Another advantage of forming PtGa alloy is the increase of the surface stability. The p–d interaction caused the Pt to be more resistant to oxidation, and the Ga to be less prone to leaching. The stability of both Pt and Ga contributed to the overall stability of the catalysts.

In terms of stability, alloy nanowires benefit from both the anisotropic morphology and the alloy nature. It is well accepted that the 1D morphology can provide more interaction points between the metal catalyst and the carbon support, helping to prevent the dissolution of the nanowires and

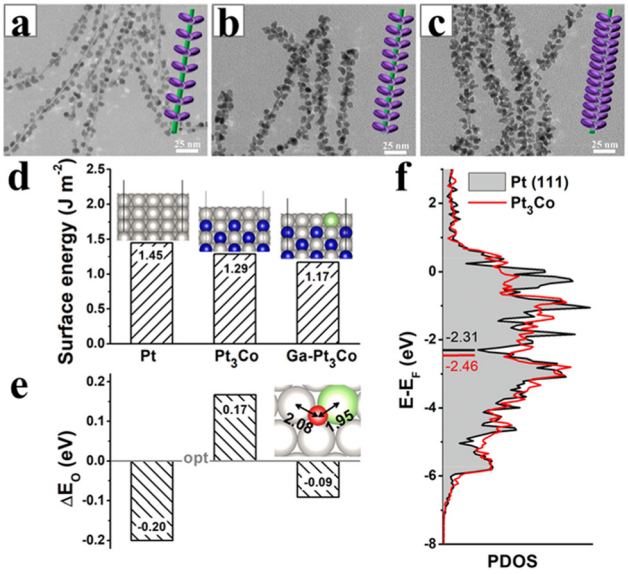

Fig. 28 (a) TEM images and schematic illustrations of (a) 2% Ga–Pt_3Co, (b) 4% Ga–Pt_3Co, and (c) 8% Ga–Pt_3Co nanowires. (d) Surface energy and (e) ΔE_O of the pure Pt, Pt_3Co, and Ga-doped Pt_3Co (111) surfaces. The optimal E_O is set to 0. The computational models are shown in insets: gray, blue, green, and red spheres represent Pt, Co, Ga, and O atoms, respectively. (f) The partial density of states (PDOS) for the 3d band of the Pt atoms in the pure Pt and Pt_3Co surfaces, respectively. The horizontal lines indicate the calculated d-band centres. Reprinted with permission from ref. 76. Copyright 2020 from the American Chemical Society.

increase the charge transfer capabilities. The alloy contributes to the chemical stability of the catalysts. For instance, it was calculated that Pt_{ML}/Pt_3Co had a decreased surface energy compared with pristine Pt, and addition of Ga would further decrease the surface energy, leading to an increase in the stability of the surface and the stability of the PtCoGa catalyst during catalytic cycles (Fig. 28).[76]

In a recent work, a leaching mechanism was proposed to explain the ultrahigh stability of twisty PtNi nanowires.[135] The nanowires would first benefit from the twisting morphology, which formed a self-tangled morphology on the electrodes, and thus made the nanowires more resistant to coalescence and detachment. Moreover, the continuous leaching of Ni in the alloy would constantly replenish the surface active sites during the catalytic process. As a result, the $E_{1/2}$ of the twisty PtNi can be maintained for almost 200 000 ORR cycles, much longer than those in normal ORR catalytic systems.

5.2 Alcohol oxidation reactions

Many Pt- and Pd-based alloys are bi-functional catalysts. They also exhibit satisfying activities for alcohol oxidation reactions (AORs), which are the important anode reactions in direct alcohol fuel cells (DAFCs). This is because the AOR catalyst needs to have a certain affinity for the oxygen species, as the catalytic AORs involve the surface dissociation of H_2O and formation of oxide species on the catalysts as the oxygen sources. Typical alcohol oxidation reactions include the methanol oxidation (MOR), ethanol oxidation (EOR), and sometimes formic acid oxidation (FAOR), ethylene glycol oxidation (EGOR) and glycerol oxidation (GOR) reactions. Among them, MOR is the most studied catalytic process. Many Pt-based alloy nanowires, including PtPd, PtPb, PtCu, PtCo, PtRu, PtIr, and ternary PtCuNi nanowires have been demonstrated as having excellent performances as MOR catalysts. It is also reported that some Pd-based nanowires and the NiCu alloy nanowires are good MOR catalysts. As the anode reaction for direct ethanol fuel cells (DEFCs), EOR reactions are also widely studied. PtAg, PtZn, PtFe and PtCuNi, PtMoNi, and the Pd-based PdAu, PdAg and PdCu alloy nanowires have been shown to have improved EOR performances.

One key concern in MOR (and also other AORs) is the elimination of the carbonaceous intermediates, typically CO_{ad}, during the oxidation reaction. CO binds strongly on the pristine Pt surface, blocking the surface active sites and deactivating the catalysts. The catalytic activity is thus compromised, as extra overpotential is required to remove the intermediates. Owing to the ligand effect of alloying, many metal alloy nanowires benefit from the reduced binding energy for the carbonaceous intermediates. For instance, the onset oxidation potential for CO_{ad} would continuously shift to the cathodic side as the Pd percentage in the AuAgPd nanowire decreased gradually, indicating the decrease of the CO adsorption energy on the catalyst surface (Fig. 29d).[48] This could be attributed to the electron donation from Au and Ag to Pd. A similar effect was observed in Pt_3Ag nanowires, and the weak affinity of Ag was also believed contribute to the weak adsorption of CO on the Pt_3Ag nanowires.[127]

In addition to lowering the adsorption of CO_{ad}, the performance of alcohol oxidation catalysts can be enhanced by promoting the adsorption of OH_{ad}, which would accelerate the oxidation kinetics and the elimination of the carbonaceous species. A strain effect was recently introduced to elevate the affinity of surface Pd towards OH_{ad}. The tensile strain in Pd, which is caused by the lattice mismatch between the AuAg and sheath Pd in the ultrathin nanowires, raised the d-band centre of Pd and increased the adsorption of OH species.[48] As a result, the highly strained AuAgPd showed superior performances in EGOR and other biomass-derived alcohol oxidations (Fig. 29).

Alternatively, some oxophilic metals can be incorporated into the metal nanowires to alter the surface affinity for OH_{ad}. In a recent work, PtCoRh ternary nanowires were reported to possess outstanding MOR activities.[74] Typically, Rh is more oxophilic than Pt, and the formation of PtRh nanowires could increase the surface adsorption of OH species. Moreover, CO_{ad} bonds to the PtRh surface in a bridge manner and was thus more easily removed.

Oxophilic main group metals can also be incorporated to tune CO adsorption and the performance of the alcohol oxidation on the Pd and Pt surface. For example, Pb can be oxidized at much lower potential. Therefore, on the surface of PtPb alloy, water dissociation occurs more easily on the Pb

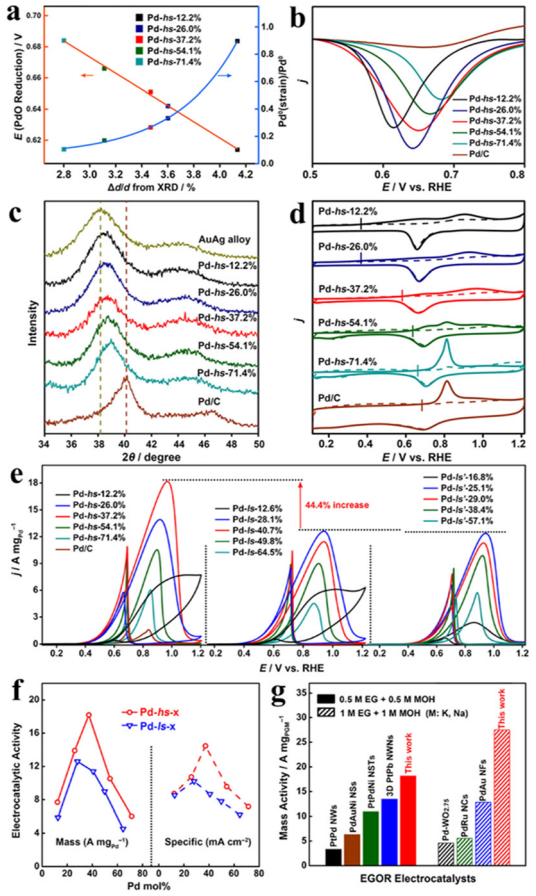

Fig. 29 Properties of the highly strained AuAgPd alloy nanowires (Pd-hs-*x*,*x* = 12.2%–71.4%). (a) The potentials of the PdO reduction peaks and the XPS area ratios of Pd^0(strain)/Pd^0 as functions of the tensile strains ($\Delta d/d$ from XRD) in the AuAgPd alloy nanowires. (b) XRD patterns of the Pd-hs-*x* nanowires. (c) PdO reduction peaks of the Pd-hs-*x* nanowires in N_2-saturated 0.5 M KOH (scan range: 0.1–1.2 V). (d) CO stripping voltammograms of the nanowires in 0.5 M KOH. Vertical bars indicate the onset potentials of the CO oxidation peaks. (e) CV curves of the Pd-hs-*x*, Pd-ls-*x*, Pd-ls'-*x* nanowires and the commercial Pd/C in 0.5 M EG + 0.5 M KOH (scan rate: 50 mV s^{-1}). (f) SA and MA of the Pd-hs-*x* and Pd-ls-*x* catalysts in the EGOR. (g) Comparison of the EGOR activity of the Pd-hs-37.2% nanowires with previously reported values. Reprinted with permission from ref. 48. Copyright 2021 from the American Chemical Society.

sites, and the resulting Pb–OH_{ad} could help to oxidize the CO_{ad} on adjacent Pt atoms. As a result, the nerve-like $Pt_{3.5}Pb$ nanowires exhibited improved MOR activity in both acidic and alkaline conditions: the SA and MA are 4.10 (1.18 A mg_{Pt}^{-1}) times and 5.24 (2.78 mA cm^{-2}) times higher than those of Pt/C in the acidic condition, and 3.45 (2.84 A mg_{Pt}^{-1}) and 4.12 (6.51 mA cm^{-2}) times higher in the alkaline condition.[111] This strategy was also employed in ultrathin PdB nanowires.[95] The incorporation of B into the nanowires was believed not only to weaken the adsorption of CO, but also facilitate the adsorption of OH.

Besides enhancing the activities of the nanowires, alloying also contributes to the stability of the catalysts. One typical case is the ultrathin PtNiMo nanowires synthesized *via* the thermal decomposition of $Mo(CO)_6$ and the H_2-assisted reduction of $Pt(acac)_2$ and $Ni(acac)_2$.[51] The ternary nanowires exhibited superior activity and durability in MOR, and the enhanced durability of the PtNiMo nanowires was attributed to the Mo incorporation. The author carried out DFT calculations and showed that Mo can stabilize the uncoordinated sites *via* the strong Mo–Pt and Mo–Ni bonds, preventing the PtNi nanowires from dissolution and diffusion. As a result, the PtNiMo alloy nanowires exhibited much better activities and stabilities compared with Pt black and Pt/C (Fig. 30).

Being a type of 1D nanostructure, many works about alloy nanowires emphasized the structural advantage of these catalysts, such as the pathway of electron and mass transport and the increased number of surface defects as active sites. Recently, further optimization of the structure factor was performed in a type of PtNiCu alloy nanowire. The exposed (110) and (100) facets in the PtNiCu nanowires increased from 36% to 88.3% after washing the as-synthesized nanowires with acetic acid.[118] Compared with (111) facets, the (110) facets possess more abundant active catalytic sites and the (100) facets have lower surface energy, which favours the desorption of CO_{ad}. The synergistic effect of the two facets led to lower onset potentials for CO_{ad} and easier oxidation of the CO_{ad} on the catalyst surface. Thus, the PtNiCu alloy nanowires after acid treatment exhibited a specific activity of 3.25 mA cm^{-2}, 2.2 and 4.5 times higher than those of PtNiCu nanowires and Pt/C.

Apart from the AORs, there were reports about applying metal alloy nanowires, such as the high-entropy

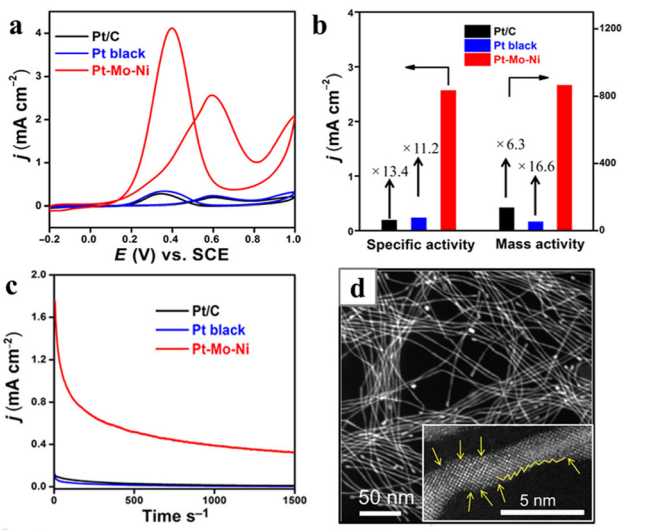

Fig. 30 Morphology and the electrochemical performance of PtNiMo alloy nanowires. (a) CVs of Pt black, Pt/C and as-prepared PtMoNi nanowires recorded in 0.5 M H_2SO_4 + 2 M CH_3CH_2OH solution at a scan rate of 50 mV s^{-1}. (b) Comparison of SAs and MAs of the three catalysts. (c) chronoamperometric curves for the three catalysts recorded at 0.5 V *versus* SCE. (d) HAADF-STEM image (inset: enlarged image) of the PtMoNi nanowires. Reprinted with permission from ref. 51. Copyright 2017 from AAAS.

PtRuNiCoFeMo nanowires, as catalysts for the hydrogen oxidation reaction (HOR), which is also an important anode reaction for fuel cells. A recent work investigated in detail the effect of Ni in the PtNi alloy nanowires for alkaline HOR.[139,186] PtNi alloy nanowires with the Ni presented either at the core or the surface of the nanowires were compared, and it was found that the surface Ni could enhance the HOR activity more significantly by increasing the adsorption of both *H and *OH species.

5.3 Water-splitting and CO_2 reduction reactions

The electrocatalytic water-splitting process produces H_2 as chemical fuel. The process involves the hydrogen evolution reaction (HER) and oxygen evolution reaction (OER). As a 1 – e^- process, the kinetics for HER is relatively fast on a Pt catalyst surface. Still, many Pt- and Pd-based nanowires have been demonstrated to be capable of further accelerating the HER kinetics.[187] For instance, the PtM–S alloy nanowires formed with SO_3^{2-} as the additive in aqueous condition had ultrathin morphology and an optimized number of surface Pt/M–S(OH) interfaces. The Pt/M–S(OH) interfaces were composed of both the oxide/sulphide sites for effective water cleavage and the Pt surface for effective formation of H_2 from the H_{ad}. Thus, the alloy nanowires showed superior activity for the HER in alkaline conditions. The MA and SA of the alloy nanowires were more than 5 times higher than that of the Pt/C.

Pt and Pd-based metal alloy nanowires have seldom been applied as OER catalysts, probably because they were out-competed by RuO_2 and IrO_2 in catalytic OER reactions. Nevertheless, the OER activity of the Ru-containing high-entropy AlNiCoRuX alloy nanowires had been demonstrated besides their HER and ORR activity.[143] It was found that the OER activities decreased when Co was added into the AlNiRu alloy, while the further incorporation of Mo yielded the AlNiRuCoMo alloy with the best OER performance. The author investigated the effect of Mo using calculation methods. By calculating the occupancies of the e_g orbital of the octahedral sites in the surface oxide with inverse spinel structure, it was concluded that Mo doping would make the e_g occupancies in both Co and Ru close to unity, leading to optimized ORR and OER activities in the quinary alloy.

Electrocatalytic reduction of CO_2 (CO_2RR) has become an emerging field in recent years, as it is one potential solution for slowing down and stopping the increase of the level of CO_2 in the atmosphere. However, CO_2RR is a complex reaction with multiple pathways and products, and must compete with HER in aqueous systems.[188–191] Thus, a catalyst is of critical importance for electrocatalytic CO_2RR, and a variety of metal-based catalysts have been developed for effective and selective CO_2RR.

On the other hand, there are only a few reports about alloy nanowires for CO_2RR applications, as Pt-based materials are more suited to the competitive HER.[192] In one recent work, AgPd (Pd_4Ag) nanowires were designed as an efficient CO_2RR catalyst, as Pd can reduce CO_2 to formate with low overpotential and high selectivity (Fig. 31).[193] Since Ag has much weaker affinity for CO, the formation of an Ag alloy would weaken the CO binding on the catalyst surface sites, therefore inhibiting the CO poisoning that usually happens in Pd-based catalysts (Fig. 31e–g). As a result, the AgPd alloy nanowire can maintain more than 90% formate selectivity until the reduction potential reaches −0.3 V (*vs.* RHE), and also exhibits long-term stability for formate production at −0.43 V (*vs.* RHE).

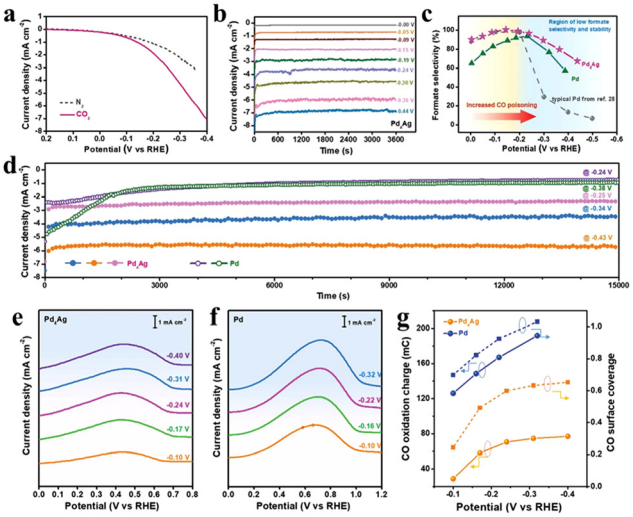

Fig. 31 CO_2RR performance of AgPd and Pd nanowires. (a) Polarization curves of Pd_4Ag in CO_2- or N_2-saturated 0.1 M $KHCO_3$. (b) Total current density of AgPd at different working potentials. (c) Potential-dependent formate selectivity of AgPd in comparison with those of pure Pd and typical Pd catalyst from the literature. (d) Long-term chronoamperometric curves of AgPd and pure Pd for 15 000 s at a few selected potentials as indicated. (e–g) Analysis of the CO accumulation on AgPd and pure Pd during CO_2RR. Positive going polarization curves on (e) AgPd and (f) pure Pd immediately after 1 h CO_2RR electrocatalysis at different working potentials as indicated; (g) integrated CO oxidation charge and corresponding CO surface coverage on AgPd and pure Pd at different working potentials. Reprinted with permission from ref. 194. Copyright 2020 from Wiley-VCH GmbH.

5.4 Other applications

Besides functioning directly as electrocatalysts, metal nanowires have been utilized in electrochemical analysis, catalytic reactions and other applications. For instance, PtNi nanowires have been assembled on reduced graphene oxide and applied as H_2O_2 sensors;[194] ultrathin PdAg nanowires were applied as glucose sensors;[195] and PdPt nanowires with excellent oxidation ability can be used for the detection of acid phosphatase in acidic conditions.[168]

PtCoFe alloy nanowires were applied as the counter electrode and boosted the efficiency of dye-sensitized solar cells.[98] Compared with pure Pt nanowires, the PtCoFe nanowires catalysed the conversion of I_3^- to I^- more efficiently. The DFT calculation showed that the (111) facets of the ternary alloy could adsorb the I_2 intermediates after the initial decomposition of the I_3^-, and facilitate the dissociation of I_2 into I^-. The theoretical result also further specified that the more active ternary alloy was $Pt_{49}Co_{23}Fe_{28}$ from the adsorption and desorption energies of I_2 on different (111) surfaces.

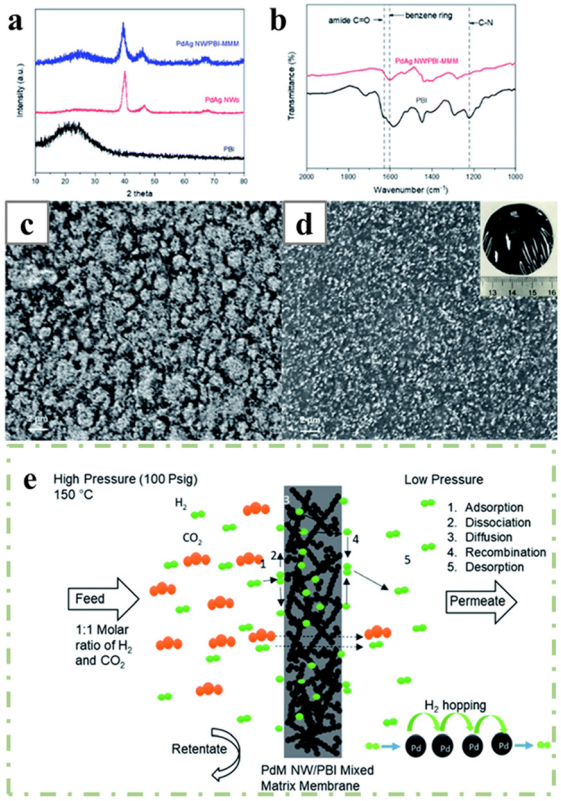

Fig. 32 (a) XRD patterns and (b) FTIR spectra of PBI and PdAg NW/PBI-MMM; SEM images of (c) bottom (d) top section of PBI-PdAg NW/PBI-MMM. Inset shows a photograph of a PdAg NW/PBI-MMM. (e) Schematic illustrating the hydrogen separation mechanism in a PdM NW-PBI MMM. Reprinted with permission from ref. 128. Copyright 2021 from the Royal Society of Chemistry.

PdM (M = Ag, Y, Ni, Cu) nanowires were recently loaded into a polybenzimidazole (PBI) membrane to form a mixed matrix membrane (MMM) with improved H_2 transportation and separation abilities (Fig. 32).[128] Since H_2 dissolves and diffuses through the metallic Pd in the form of H atoms, the PdM nanowires in the membrane can form continuous highways for the transportation of H_2 through the membrane. The addition of alloy metal would further increase the permeability of H and in the meantime reduce consumption of the expensive Pd. On the other hand, CO_2, the other product of steam reforming, can only diffuse through the PBI blocks. As a result, the MMM showed an impressive separation ability compared with the polymer membranes.

Some alloy nanowires were shown to be highly active in certain organic reactions. For example, PtFe nanowires can facilitate the selective and efficient hydrogenation of acetophenone and yield more than 90% of 1-phenylethanol at 99.3% conversion at 200 min.[196] Both the activity and the selectivity of the alloy nanowires were much better than that of the pure Pt nanowires as well as the PtFe nanocubes. The high activity and selectivity of the alloy were attributed to the electron transfer from Pt and Fe, which produced electron-deficient surface Pt sites that are more favourable to the C=O groups. Moreover, the nanowire morphology leads to various high-index surface facets, as compared with the cubic PtFe. The stepped sites on the high-index facets would prefer the adsorption of C=O over the aromatic rings, while both groups would be adsorbed on the cubic facets, leading to the improved selectivity on the nanowires.

In summary, metal alloy nanowires have diverse applications in electrocatalysis owing to the numerous metal combinations. Pt- and Pd-based nanowires have been investigated as advanced ORR, AOR and HER catalysts, as alloying could further optimize the electronic structures of the Pt and Pd and improve the catalytic performances. Nanowires containing Ru or Ir may be applied as OER catalyst, and the non-noble metals like Co and Ni are also active for this reaction. The electrocatalytic CO_2 reduction, on the other hand, is to some extent underexplored at this moment. The Au and Ag-based materials usually have high selectivity for CO, and Cu is current the only metal that can facilitate the formation of the C–C bond in CO_2RR. Therefore, it is desirable to synthesize and investigate the CO_2RR properties of nanowires made of these metals.

6. Conclusions and outlook

This work focuses mainly on the chemical syntheses of alloy, mostly noble metal-based, nanowires in recent years. Both the morphological control and the composition adjustment need to be considered in the synthesis of metal alloy nanowires. In order to achieve growth of the 1D nanostructure, the alloy nanowires can either be formed directly or *via* the post-synthetic processing of pristine metal nanowires. The latter can also be considered as a type of templating method, with the metal nanowires as the templating precursors, while the former method involves the co-reduction and precipitation of multiple precursors under certain chemical conditions.

Many methods that directly grow alloy nanowires have been developed from the syntheses of the pristine metal nanowires. Despite various compositions, alloy nanowires and the corresponding synthesis of the pristine nanowires share the same or similar mechanism for 1D growth, such as templating methods, ligand-direct deposition and elongation, and oriented attachment. Nevertheless, given the various reduction potentials of the metal ions, modifications to the syntheses need to be imposed to enable the co-reduction of the metal precursors. The autocatalytic effect of Pt plays an important role in many Pt-based syntheses, leading to the formation of a large variety of Pt-based nanowires. Furthermore, additional reducing agents with strong reducing abilities are required to create a more reductive environment for non-noble metals. Sometimes, less reactive precursors or additional coordination ligands were introduced to overcome the differences in the reduction potentials.

The methods based on existing nanowires can be divided into two categories: displacement-based methods and those without displacement reactions. The latter rely largely on the interdiffusion of the atoms to form the alloy nanowires.

Typically, the interdiffusion can occur easily in ultrathin nanowires, resulting in a thorough mixing of the metal atoms and homogeneous phases in the alloy nanowires. In the relatively thicker nanowires, interdiffusion would encounter a kinetics problem, resulting in only surface doping. The thermal annealing process can help to initiate the interdiffusion and formation of homogeneous crystalline phases, while protection layers may be required for ultrathin nanowires to maintain the morphology during the high-temperature processes. In contrast, syntheses with template nanowires made of metals with low reduction potentials usually involve displacement reactions between the templates and the growth materials. These methods often produce tubular structures, as the displacement is always initiated from the nanowire surfaces.

Applications of metal alloy nanowires were also briefly reviewed. The metal alloy nanowires all exhibited improved catalytic properties, demonstrating the advantages of this group of materials. Many works discussed the compositional advantages of the alloys: the strain effect and the ligand effect of the alloy formation alter (or optimize) the electronic structure of the nanomaterials, making the surface more favourable to heterogeneous catalytic processes. Computational works, such as DFT calculations, were sometimes employed to articulate the effect in detail. Generally, the Pt or Pd composition in the alloy is still considered as the active site for catalytic processes, and the d band centre of the surface Pt/Pd and the adsorption energies on the surface Pt/Pd are varied by the alloying metals.

Although a variety of metal alloy nanowires have been synthesized and investigated, there remain plenty of challenges in this field. First, exploration of new routes or approaches to the synthesis of nanowires remains highly desirable. Synthesis is the foundation of all applications. Increase of the composition and structural diversities in the alloy nanowires would provide larger material reservoirs for customized applications. On the other hand, although a variety of synthetic protocols have been developed in the past several decades, ligand systems that are compatible with both inducing 1D growth and accommodating mixing of different metals are still quite limited.

In terms of understanding the syntheses, although the majority of the reported works provided studies on the growth processes, the underlying formation mechanisms for many 1D structures remain largely unclear. For example, many works attributed the formation of the 1D nanostructures to the oriented attachment mechanism, while the motivation as well as the step-by-step procedures for the oriented attachment process are to some extent underexplored: metal crystals are highly symmetric, and a symmetry-breaking mechanism would be required to drive the 1D assembly. Furthermore, the exact roles of the structural-directing reagents in many solution-based chemical processes were not specified. For instance, both CO and PVP have been reported as being able to induce the formation of Pt-based nanowires, yet the morphologies of the nanowires obtained with CO reagents are distinctively different from those induced by PVP. Therefore, it is quite unlikely that the two species take effect in a similar way. Cutting-edge characterization techniques such as *in situ* TEM might be able to provide additional insights into the growth mechanism and properties,[197] while systematic and ingenious design of the control experiments would also be helpful for logical deductions.

There is still plenty of room for new alloy materials. Bimetallic alloy nanowires remain to be the most commonly synthesized 1D nanostructures. Forming alloys with more metals would definitely create materials with more diverse properties. And, of course, this would add to the complexities of the synthesis. Also, the compositions of the alloy nanowires need to be better controlled and characterized. Currently, the compositions of many metal alloy nanowires are adjusted by varying the feeding ratios of the metal precursors, and sometimes the metal ratio in the final nanowires deviates from the feeding ratios. Although characterizations such as EDS mapping were provided in almost all works, the microscopic distribution of the metal atoms remains largely unclear, except for those forming alloy crystal with determining phases. This uncertainty would compromise the validity of the theoretical calculations, and also cause difficulties in identifying the structure–property correlations.

Finally, being an additional dimension to tuning the chemical and physical properties of nanostructures, phase engineering has drawn increasing attention in recent years. A series of nanostructures containing metastable phases have been synthesized and demonstrated to have excellent electrocatalytic activities.[198,199] Nanowires with high strain phases have been reported in some works, and the investigation of phase-dependent activities in alloy nanowires has just began.

Author contributions

S. Li, H. Jin and Y. Wang conceived the idea. Y. Wang wrote the original draft, S. Li and H. Jin completed the reproduction of figures. S. Li and Y. Wang revised the manuscript.

Conflicts of interest

There are no conflicts to declare.

Acknowledgements

We gratefully acknowledge financial support from the National Natural Science Foundation of China (21703104), Jiangsu Science and Technology Plan (BK20170980), and Nanjing Tech University (39837131).

References

1 M. Aneke and M. Wang, *Appl. Energy*, 2016, **179**, 350–377.
2 S. Koohi-Fayegh and M. A. Rosen, *J. Energy Storage*, 2020, **27**, 101047.

3 A. Evans, V. Strezov and T. J. Evans, *Renewable Sustainable Energy Rev.*, 2012, **16**, 4141–4147.
4 T. M. I. Mahlia, T. J. Saktisahdan, A. Jannifar, M. H. Hasan and H. S. C. Matseelar, *Renewable Sustainable Energy Rev.*, 2014, **33**, 532–545.
5 T. Kousksou, P. Bruel, A. Jamil, T. El Rhafiki and Y. Zeraouli, *Sol. Energy Mater. Sol. Cells*, 2014, **120**, 59–80.
6 O. Z. Sharaf and M. F. Orhan, *Renewable Sustainable Energy Rev.*, 2014, **32**, 810–853.
7 H. Xie, T. Wang, J. Liang, Q. Li and S. Sun, *Nano Today*, 2018, **21**, 41–54.
8 P. E. Dodds, I. Staffell, A. D. Hawkes, F. Li, P. Grünewald, W. McDowall and P. Ekins, *Int. J. Hydrogen Energy*, 2015, **40**, 2065–2083.
9 R. Sharifian, R. M. Wagterveld, I. A. Digdaya, C. Xiang and D. A. Vermaas, *Energy Environ. Sci.*, 2021, **14**, 781–814.
10 B. Zhang, Y. Jiang, M. Gao, T. Ma, W. Sun and H. Pan, *Nano Energy*, 2021, **80**, 105504.
11 A. Eftekhari and B. Fang, *Int. J. Hydrogen Energy*, 2017, **42**, 25143–25165.
12 H. Chen, Y. S. Zhou, W. Guo and B. Y. Xia, *Chin. Chem. Lett.*, 2022, **33**, 1831–1840.
13 F. Y. Shi, L. L. Zhai, Q. Q. Liu, J. Y. Yu, S. P. Lau, B. Y. Xia and Z. L. Xu, *J. Energy Chem.*, 2023, **76**, 127–145.
14 H. Shen, T. Peppel, J. Strunk and Z. Sun, *Sol. RRL*, 2020, **4**, 1900546.
15 L. Sun, V. Reddu, A. C. Fisher and X. Wang, *Energy Environ. Sci.*, 2020, **13**, 374–403.
16 J. Mohammed-Ibrahim and X. Sun, *J. Energy Chem.*, 2019, **34**, 111–160.
17 M.-I. Jamesh and X. Sun, *J. Power Sources*, 2018, **400**, 31–68.
18 X. Li, X. Hao, A. Abudula and G. Guan, *J. Mater. Chem. A*, 2016, **4**, 11973–12000.
19 H. Sun, Z. Yan, F. Liu, W. Xu, F. Cheng and J. Chen, *Adv. Mater.*, 2020, **32**, 1806326.
20 T. K. Kormilina, E. A. Stepanidenko, S. A. Cherevkov, A. Dubavik, M. A. Baranov, A. V. Fedorov, A. V. Baranov, Y. K. Gun'ko and E. V. Ushakova, *J. Mater. Chem. C*, 2018, **6**, 5278–5285.
21 H. M. An, Z. L. Zhao, L. Y. Zhang, Y. Chen, Y. Y. Chang and C. M. Li, *ACS Appl. Mater. Interfaces*, 2018, **10**, 41293–41298.
22 L. Jin, H. Xu, C. Chen, H. Shang, Y. Wang, C. Wang and Y. Du, *ACS Appl. Mater. Interfaces*, 2019, **11**, 42123–42130.
23 H. Xu, F. Ren, B. Yan, J. Wang, S. Li and Y. Du, *J. Electroanal. Chem.*, 2018, **811**, 37–45.
24 F. Gao, Y. Zhang, H. You, Z. Li, B. Zou and Y. Du, *Small*, 2021, **17**, e2101428.
25 D. Huo, M. J. Kim, Z. H. Lyu, Y. F. Shi, B. J. Wiley and Y. N. Xia, *Chem. Rev.*, 2019, **119**, 8972–9073.
26 R. S. Devan, R. A. Patil, J. H. Lin and Y. R. Ma, *Adv. Funct. Mater.*, 2012, **22**, 3326–3370.
27 H. Xu, H. Y. Shang, C. Wang and Y. K. Du, *Adv. Funct. Mater.*, 2020, **30**, 2000793.
28 A. Kumar, M. M. Mohammadi and M. T. Swihart, *Nanoscale*, 2019, **11**, 19058–19085.
29 Y. Zhang, F. Gao, H. You, Z. Li, B. Zou and Y. Du, *Coord. Chem. Rev.*, 2022, **450**, 214244.
30 Y. Wang, Y. Yuan and H. Huang, *Chin. J. Chem.*, 2021, **39**, 1389–1396.
31 J. Lai and S. Guo, *Small*, 2017, **13**, 1702156.
32 Q. Shao, K. Lu and X. Huang, *Small Methods*, 2019, **3**, 1800545.
33 F. Gao, Y. Zhang, Z. Wu, H. You and Y. Du, *Coord. Chem. Rev.*, 2021, **436**, 213825.
34 P. Li and W. Chen, *Chin. J. Catal.*, 2019, **40**, 4–22.
35 L. Zhang, Z. Xie and J. Gong, *Chem. Soc. Rev.*, 2016, **45**, 3916–3934.
36 V. Stamenkovic, B. S. Mun, K. J. J. Mayrhofer, P. N. Ross, N. M. Markovic, J. Rossmeisl, J. Greeley and J. K. Norskov, *Angew. Chem., Int. Ed.*, 2006, **45**, 2897–2901.
37 M. Zhou, C. Li and J. Y. Fang, *Chem. Rev.*, 2021, **121**, 736–795.
38 Y. Nakaya and S. Furukawa, *Chem. Rev.*, 2022, **89**, Article ASAP, DOI: **10.1021/acs.chemrev.2c00356**.
39 L. Z. Bu, J. B. Ding, S. J. Guo, X. Zhang, D. Su, X. Zhu, J. L. Yao, J. Guo, G. Lu and X. Q. Huang, *Adv. Mater.*, 2015, **27**, 7204–7202.
40 T. Wang, A. Chutia, D. J. L. Brett, P. R. Shearing, G. He, G. Chai and I. P. Parkin, *Energy Environ. Sci.*, 2021, **14**, 2639–2669.
41 D. Kim, J. Resasco, Y. Yu, A. M. Asiri and P. Yang, *Nat. Commun.*, 2014, **5**, 4948.
42 J. Fan, H. Du, Y. Zhao, Q. Wang, Y. Liu, D. Li and J. Feng, *ACS Catal.*, 2020, **10**, 13560–13583.
43 L. Y. Zhang, C. X. Guo, H. J. Cao, S. Wang, Y. R. Ouyang, B. H. Xu, P. Z. Guo and C. M. Li, *Chem. Eng. J.*, 2022, **431**, 133237.
44 J. W. M. Crawley, I. E. Gow, N. Lawes, I. Kowalec, L. Kabalan, C. R. A. Catlow, A. J. Logsdail, S. H. Taylor, N. F. Dummer and G. J. Hutchings, *Chem. Rev.*, 2022, **122**, 6795–6849.
45 F. Gao, Y. Zhang, F. Ren, Y. Shiraishi and Y. Du, *Adv. Funct. Mater.*, 2020, **30**, 2000255.
46 X. H. Song, X. Y. Zhang, Q. Chang, X. Yao, M. F. Li, R. P. Zhang, X. T. Liu, C. Y. Song, Y. X. A. Ng, E. H. Ang and Z. H. Ou, *Small*, 2022, **18**, 2203310.
47 D. B. Williams and C. B. Carter, *Transmission Electron Microscopy A Textbook for Materials Science*, Springer, Springer New York, New York, 2009.
48 S. Zhang, K. Liu, Z. Liu, M. Liu, Z. Zhang, Z. Qiao, L. Ming and C. Gao, *Nano Lett.*, 2021, **21**, 1074–1082.
49 W. Zhang, Y. Yang, B. Huang, F. Lv, K. Wang, N. Li, M. Luo, Y. Chao, Y. Li, Y. Sun, Z. Xu, Y. Qin, W. Yang, J. Zhou, Y. Du, D. Su and S. Guo, *Adv. Mater.*, 2019, **31**, e1805833.
50 D. E. Ramaker and C. Roth, X-ray absorption near edge structure (Δμ XANES) techniques for low temperature fuel cell characterization, in *Polymer Electrolyte Membrane and Direct Methanol Fuel Cell Technology*, 2012, pp. 120–145.

51 J. J. Mao, W. X. Chen, D. S. He, J. W. Wan, J. J. Pei, J. C. Dong, Y. Wang, P. F. An, Z. Jin, W. Xing, H. L. Tang, Z. B. Zhuang, X. Liang, Y. Huang, G. Zhou, L. Y. Wang, D. S. Wang and Y. D. Li, *Sci. Adv.*, 2017, **3**, 323–324.
52 D. Shore, A. Ghemes, O. Dragos-Pinzaru, Z. Gao, Q. Shao, A. Sharma, J. Um, I. Tabakovic, J. C. Bischof and B. J. H. Stadler, *Nanoscale*, 2019, **11**, 14607–14615.
53 S. Khan, N. Ahmad, N. Ahmed and X. F. Han, *J. Magn. Magn. Mater.*, 2018, **460**, 120–127.
54 J. C. Xu, B. Hong, X. L. Peng, X. Q. Wang, H. L. Ge and J. Hu, *Chem. Phys. Lett.*, 2021, **767**, 138368.
55 S. Samanifar, M. A. Kashi and A. Ramazani, *Phys. C*, 2018, **548**, 72–74.
56 L. Du, D. Feng, X. Xing, C. Wang, G. S. Armatas and D. Yang, *Chem. Eng. J.*, 2020, **400**, 125864.
57 L. Du, L. Zheng, H. Wei, S. Zheng, Z. Zhu, J. Chen and D. Yang, *ACS Appl. Nano Mater.*, 2019, **2**, 1178–1184.
58 J. S. Riva, A. V. Juárez, S. E. Urreta and L. M. Yudi, *Electrochim. Acta*, 2019, **298**, 379–388.
59 C. Wang, L. Zheng, R. Chang, L. Du, C. Zhu, D. Geng and D. Yang, *ACS Appl. Mater. Interfaces*, 2018, **10**, 29965–29971.
60 D. Li and E. J. Podlaha, *Nano Lett.*, 2019, **19**, 3569–3574.
61 P. Zhang, I. Wyman, J. Hu, S. Lin, Z. Zhong, Y. Tu, Z. Huang and Y. Wei, *Mater. Sci. Eng., B*, 2017, **223**, 1–23.
62 X. Li, Y. Wang, C. Yin and Z. Yin, *J. Mater. Chem. C*, 2020, **8**, 849–872.
63 S. Fahad, H. Yu, L. Wang, Zain-ul-Abdin, M. Haroon, R. S. Ullah, A. Nazir, K.-u.-R. Naveed, T. Elshaarani and A. Khan, *J. Mater. Sci.*, 2018, **54**, 997–1035.
64 N. A. C. Lah and S. Trigueros, *Sci. Technol. Adv. Mater.*, 2019, **20**, 225–261.
65 L. Bu, J. Ding, S. Guo, X. Zhang, D. Su, X. Zhu, J. Yao, J. Guo, G. Lu and X. Huang, *Adv. Mater.*, 2015, **27**, 7204–7212.
66 K. Jiang, Q. Shao, D. Zhao, L. Bu, J. Guo and X. Huang, *Adv. Funct. Mater.*, 2017, **27**, 1700830.
67 H. Tang, Y. Su, B. Chi, J. Zhao, D. Dang, X. Tian, S. Liao and G.-R. Li, *Chem. Eng. J.*, 2021, **418**, 129322.
68 P. Lv, B. Jin, C. Mei, H. Zhou, T. Yuan, Z. Li, H. He, X. Shen and X. Hong, *Chemistry*, 2018, **24**, 14636–14638.
69 P. Wang, X. Zhang, J. Zhang, S. Wan, S. Guo, G. Lu, J. Yao and X. Huang, *Nat. Commun.*, 2017, **8**, 14580.
70 M. Luo, Y. Sun, Y. Qin, S. Chen, Y. Li, C. Li, Y. Yang, D. Wu, N. Xu, Y. Xing, L. Wang, P. Gao and S. Guo, *Chem. Mater.*, 2018, **30**, 6660–6667.
71 L. Bu, S. Guo, X. Zhang, X. Shen, D. Su, G. Lu, X. Zhu, J. Yao, J. Guo and X. Huang, *Nat. Commun.*, 2016, **7**, 11850.
72 M. Luo, Y. Sun, X. Zhang, Y. Qin, M. Li, Y. Li, C. Li, Y. Yang, L. Wang, P. Gao, G. Lu and S. Guo, *Adv. Mater.*, 2018, **30**, 1705515.
73 Y. Xu, X. Cui, S. Wei, Q. Zhang, L. Gu, F. Meng, J. Fan and W. Zheng, *Nano Res.*, 2019, **12**, 1173–1179.
74 X. Chen, W. Wang, X. Chen, X. Liao, Z. Lyu, K. Liu and S. Xie, *Nanoscale*, 2021, **13**, 2632–2638.
75 H. Li, Y. Pan, D. Zhang, Y. Han, Z. Wang, Y. Qin, S. Lin, X. Wu, H. Zhao, J. Lai, B. Huang and L. Wang, *J. Mater. Chem. A*, 2020, **8**, 2323–2330.
76 M. Li, Z. Zhao, Z. Xia, Y. Yang, M. Luo, Y. Huang, Y. Sun, Y. Chao, W. Yang, W. Yang, Y. Yu, G. Lu and S. Guo, *ACS Catal.*, 2020, **10**, 3018–3026.
77 P. T. Wang, Q. Shao, X. N. Cui, X. Zhu and X. Q. Huang, *Adv. Funct. Mater.*, 2018, **28**, 1705918.
78 C. Zhan, Y. Xu, L. Bu, H. Zhu, Y. Feng, T. Yang, Y. Zhang, Z. Yang, B. Huang, Q. Shao and X. Huang, *Nat. Commun.*, 2021, **12**, 6261.
79 Y. Xin, S. H. Li, Y. Y. Qian, W. K. Zhu, H. B. Yuan, P. Y. Jiang, R. H. Guo and L. B. Wang, *ACS Catal.*, 2020, **10**, 11280–11306.
80 X. Wang, W. Guo and Y. Z. Fu, *J. Mater. Chem. A*, 2021, **9**, 663–701.
81 C. Chen, H. Xu, H. Shang, L. Jin, T. Song, C. Wang, F. Gao, Y. Zhang and Y. Du, *Nanoscale*, 2019, **11**, 20090–20095.
82 L. Huang, W. Zhang, Y. Zhong, P. Li, D. Xiang, W. Uddin, X. Li, Y.-G. Wang, X. Yuan, D. Wang and M. Zhu, *Sci. China Mater.*, 2020, **64**, 601–610.
83 X. L. Tian, X. Zhao, Y. Q. Su, L. J. Wang, H. M. Wang, D. Dang, B. Chi, H. F. Liu, E. J. M. Hensen, X. W. Lou and B. Y. Xia, *Science*, 2019, **366**, 850–856.
84 F. Gao, Y. Zhang, P. Song, J. Wang, B. Yan, Q. Sun, L. Li, X. Zhu and Y. Du, *Nanoscale*, 2019, **11**, 4831–4836.
85 Y. Mo, S. Feng, T. Yu, J. Chen, G. Qian, L. Luo and S. Yin, *J. Colloid Interface Sci.*, 2022, **607**, 1928–1935.
86 P. Song, H. Xu, J. Wang, Y. Zhang, F. Gao, J. Guo, Y. Shiraishi and Y. Du, *Nanoscale*, 2018, **10**, 16468–16473.
87 K. Z. Jiang, D. D. Zhao, S. J. Guo, X. Zhang, X. Zhu, J. Guo, G. Lu and X. Q. Huang, *Sci. Adv.*, 2017, **3**, 1601705.
88 N. Cheng, L. Zhang, Y. Zhou, S. Yu, L. Chen, H. Jiang and C. Li, *J. Colloid Interface Sci.*, 2020, **572**, 170–178.
89 L. Huang, X. Zhang, Q. Wang, Y. Han, Y. Fang and S. Dong, *J. Am. Chem. Soc.*, 2018, **140**, 1142–1147.
90 X. Xu, H. Lv, L. Sun, P. Song, B. Liu and X. Chen, *ChemPlusChem*, 2020, **85**, 970–976.
91 H. Lv, X. Chen, D. Xu, Y. Hu, H. Zheng, S. L. Suib and B. Liu, *Appl. Catal., B*, 2018, **238**, 525–532.
92 D. Xu, X. Liu, M. Han and J. Bao, *Chem. Commun.*, 2016, **52**, 12996–12999.
93 H. Lv, L. Sun, D. Xu, Y. Ma and B. Liu, *Appl. Catal., B*, 2019, **253**, 271–277.
94 N. Han, M. Sun, Y. Zhou, J. Xu, C. Cheng, R. Zhou, L. Zhang, J. Luo, B. Huang and Y. Li, *Adv. Mater.*, 2021, **33**, 2005821.
95 Y. Wang, H. Lv, L. Sun, X. Guo, D. Xu and B. Liu, *ACS Appl. Mater. Interfaces*, 2021, **13**, 17599–17607.
96 W. L. Pei, C. Wu, Y. Zhang, Q. Wang, C. S. He, J. J. Wang, K. H. Zhang and X. Zhao, *Int. J. Nanotechnol.*, 2016, **13**, 801–808.
97 S. Guo, D. Li, H. Zhu, S. Zhang, N. M. Markovic, V. R. Stamenkovic and S. Sun, *Angew. Chem., Int. Ed.*, 2013, **52**, 3465–3468.

98 C.-C. P. Chiang, C.-Y. Hung, S.-W. Chou, J.-J. Shyue, K.-Y. Cheng, P.-J. Chang, Y.-Y. Yang, C.-Y. Lin, T.-K. Chang, Y. Chi, H.-L. Chou and P.-T. Chou, *Adv. Funct. Mater.*, 2018, **28**, 1703282.
99 H. Zhu, S. Zhang, D. Su, G. Jiang and S. Sun, *Small*, 2015, **11**, 3545–3549.
100 Z. Yang, H. Yang, L. Shang and T. Zhang, *Angew. Chem., Int. Ed.*, 2022, **61**, e202113278.
101 H. J. Yu, T. Q. Zhou, Z. Q. Wang, Y. Xu, X. N. Li, L. Wang and H. J. Wang, *Angew. Chem., Int. Ed.*, 2021, **60**, 12027–12031.
102 T. T. Zeng, X. M. Meng, H. W. Huang, L. W. Zheng, H. B. Chen, Y. Zhang, W. Y. Yuan and L. Y. Zhang, *Small*, 2022, **18**, 8.
103 J. Li, Z. Y. Zhou, H. Xu, C. Wang, S. Hata, Z. X. Dai, Y. Shiraishi and Y. K. Du, *J. Colloid Interface Sci.*, 2022, **611**, 523–532.
104 H. Ali, H. Lin, Q. Lu and X. Wang, *J. Phys. Chem. C*, 2021, **125**, 14646–14655.
105 S. Mourdikoudis and L. M. Liz-Marzán, *Chem. Mater.*, 2013, **25**, 1465–1476.
106 Z. Y. Huo, C. K. Tsung, W. Y. Huang, X. F. Zhang and P. D. Yang, *Nano Lett.*, 2008, **8**, 2041–2044.
107 C. Wang, Y. J. Hu, C. M. Lieber and S. H. Sun, *J. Am. Chem. Soc.*, 2008, **130**, 8902–8903.
108 X. Hong, Z. Yin, Z. Fan, Y. Y. Tay, J. Chen, Y. Du, C. Xue, H. Chen and H. Zhang, *Small*, 2014, **10**, 479–482.
109 R. Mendoza-Cruz, L. Bazán-Díaz, J. Jesús Velázquez-Salazar, G. Plascencia-Villa, D. Bahena-Uribe, J. Reyes-Gasga, D. Romeu, G. Guisbiers, R. Herrera-Becerra and M. José-Yacamán, *Nano Lett.*, 2016, **16**, 1568–1573.
110 Y. Imura, T. Mori, C. Morita-Imura, H. Kataoka, R. Akiyama, H. Kurata and T. Kawai, *Colloids Surf., A*, 2018, **543**, 9–14.
111 L. Huang, Y. Han, X. Zhang, Y. Fang and S. Dong, *Nanoscale*, 2017, **9**, 201–207.
112 F. Chang, Z. Bai, M. Li, M. Ren, T. Liu, L. Yang, C. J. Zhong and J. Lu, *Nano Lett.*, 2020, **20**, 2416–2422.
113 M. Ren, F. Chang, R. Miao, X. He, L. Yang, X. Wang and Z. Bai, *Inorg. Chem. Front.*, 2020, **7**, 1713–1718.
114 M. Gong, Z. Deng, D. Xiao, L. Han, T. Zhao, Y. Lu, T. Shen, X. Liu, R. Lin, T. Huang, G. Zhou, H. Xin and D. Wang, *ACS Catal.*, 2019, **9**, 4488–4494.
115 X. Zhai, P. Wang, K. Wang, J. Li, X. Pang, X. Wang and Z. Li, *Ionics*, 2020, **26**, 3091–3097.
116 Q. Lu, L. Sun, X. Zhao, J. Huang, C. Han and X. Yang, *Nano Res.*, 2018, **11**, 2562–2572.
117 M. Li, Y. Wang, J. Cai, Y. Li, Y. Liu, Y. Dong, S. Li, X. Yuan, X. Zhang and X. Dai, *Dalton Trans.*, 2020, **49**, 13999–14008.
118 S. Li, Y. Wang, Y. Li, X. Fang, Y. Liu, M. Li, Z. Wang, Y. Gao, H. Sun, F. Gao, X. Zhang and X. Dai, *Nano Res.*, 2021, **15**, 2877–2886.
119 Z. Lin, Y. Sheng, J. Li, Z. Rui, Y. Liu, J. Liu and Z. Zou, *Chem. Commun.*, 2020, **56**, 4276–4279.
120 B. Y. Xia, H. B. Wu, Y. Yan, X. W. Lou and X. Wang, *J. Am. Chem. Soc.*, 2013, **135**, 9480–9485.
121 F. Chang, J. Wei, Q. Zhang, Z. Jia, Y. Liu, L. Yang, X. Wang and Z. Bai, *Mater. Chem. Front.*, 2021, **5**, 8118–8126.
122 S. Liu, H. Ren, S. Yin, H. Zhang, Z. Wang, Y. Xu, X. Li, L. Wang and H. Wang, *Chem. Eng. J.*, 2022, **435**, 134823.
123 S. Liu, S. Yin, Z. Wang, Y. Xu, X. Li, L. Wang and H. Wang, *Cell Rep. Phys. Sci.*, 2022, **3**, 100869.
124 Z.-J. Wang, X. Wang, J.-J. Lv, J.-J. Feng, X. Xu, A.-J. Wang and Z. Liang, *New J. Chem.*, 2017, **41**, 3894–3899.
125 X. Jiang, G. T. Fu, X. Wu, Y. Liu, M. Y. Zhang, D. M. Sun, L. Xu and Y. W. Tang, *Nano Res.*, 2018, **11**, 499–510.
126 Y. Wang, Q. Wang, H. Sun, W. Zhang, G. Chen, Y. Wang, X. Shen, Y. Han, X. Lu and H. Chen, *J. Am. Chem. Soc.*, 2011, **133**, 20060–20063.
127 X. Fu, C. Wan, A. Zhang, Z. Zhao, H. Huyan, X. Pan, S. Du, X. Duan and Y. Huang, *Nano Res.*, 2020, **13**, 1472–1478.
128 A. Kumar, L. Huang, L. Hu, D. Yin, H. Lin and M. T. Swihart, *J. Mater. Chem. A*, 2021, **9**, 12755–12762.
129 H. You, F. Gao, C. Wang, J. Li, K. Zhang, Y. Zhang and Y. Du, *Nanoscale*, 2021, **13**, 17939–17944.
130 Y. Gong, X. Liu, Y. Gong, D. Wu, B. Xu, L. Bi, L. Y. Zhang and X. S. Zhao, *J. Colloid Interface Sci.*, 2018, **530**, 189–195.
131 B. Yan, H. Xu, K. Zhang, S. Li, J. Wang, Y. Shi and Y. Du, *Appl. Surf. Sci.*, 2018, **434**, 701–710.
132 D. Sun, H. Yu, H. Su, F. Jin, J. Liu and C. C. Li, *ChemCatChem*, 2017, **9**, 347–353.
133 H. Liu, Y. S. Yu, W. W. Yang, W. J. Lei, M. Y. Gao and S. J. Guo, *Nanoscale*, 2017, **9**, 9305–9309.
134 H. Liu, X. Y. Liu, Y. S. Yu, W. W. Yang, J. Li, M. Feng and H. B. Li, *J. Mater. Chem. A*, 2018, **6**, 4611–4616.
135 L. Sahoo, R. Garg, K. Kaur, C. P. Vinod and U. K. Gautam, *Nano Lett.*, 2022, **22**, 246–254.
136 Z. Zhang, M. Xie, Z. Liu, Y. Lu, S. Zhang, M. Liu, K. Liu, T. Cheng and C. Gao, *ACS Appl. Energy Mater.*, 2021, **4**, 6824–6832.
137 L. Wu, Z. Liu, M. Xu, J. Zhang, X. Yang, Y. Huang, J. Lin, D. Sun, L. Xu and Y. Tang, *Int. J. Hydrogen Energy*, 2016, **41**, 6805–6813.
138 H. Lv, L. Sun, D. Xu and B. Liu, *Sci. Bull.*, 2020, **65**, 1823–1831.
139 X. Li, K. X. Yao, F. Zhao, X. Yang, J. Li, Y. Li and Q. Yuan, *Nano Res.*, 2022, **15**, 6036–6044.
140 J. J. Lv, Z. J. Wang, J. J. Feng, R. h. Qiu, A. J. Wang and X. h. Xu, *Appl. Catal., A*, 2016, **522**, 188–193.
141 R. L. Zhang, J. J. Feng, L. Zhang, C. G. Shi and A. J. Wang, *J. Colloid Interface Sci.*, 2019, **555**, 276–283.
142 B. Luo, F. Zhao, Z. Xie, Q. Yuan, F. Yang, X. Yang, C. Li and Z. Zhou, *ACS Appl. Mater. Interfaces*, 2019, **11**, 32282–32290.
143 Z. Y. Jin, J. Lyu, Y. L. Zhao, H. L. Li, X. Lin, G. Q. Xie, X. J. Liu, J. J. Kai and H. J. Qiu, *ACS Mater. Lett.*, 2020, **2**, 1698–1706.
144 J. X. Tang, Q. S. Chen, L. X. You, H. G. Liao, S. G. Sun, S. G. Zhou, Z. N. Xu, Y. M. Chen and G. C. Guo, *J. Mater. Chem. A*, 2018, **6**, 2327–2336.

145 X. Yuan, M. S. Riaz, X. Wang, C. Dong, Z. Zhang and F. Huang, *Chemistry*, 2018, **24**, 3707–3711.
146 Q. Xue, X. Y. Bai, Y. Zhao, Y. N. Li, T. J. Wang, H. Y. Sun, F. M. Li, P. Chen, P. Jin, S. B. Yin and Y. Chen, *J. Energy Chem.*, 2022, **65**, 94–102.
147 D. Wu, W. Zhang and D. Cheng, *ACS Appl. Mater. Interfaces*, 2017, **9**, 19843–19851.
148 N. Zhang, Y. Zhu, Q. Shao, X. Zhu and X. Huang, *J. Mater. Chem. A*, 2017, **5**, 18977–18983.
149 X. Jiang, Y. Xiong, R. Zhao, J. Zhou, J.-M. Lee and Y. Tang, *Nano Res.*, 2020, **13**, 2691–2696.
150 J. Wang, X. Zhang, M. Zhang, P. Zhang, Y. Song and J. Zhang, *Mater. Lett.*, 2021, **305**, 130823.
151 D. Fan, K. Guo, Q. Hao, Y. Zhang and D. Xu, *Chem. Commun.*, 2022, **58**, 7773–7776.
152 L. Gao, X. X. Li, Z. Y. Yao, H. J. Bai, Y. F. Lu, C. Ma, S. F. Lu, Z. M. Peng, J. L. Yang, A. L. Pan and H. W. Huang, *J. Am. Chem. Soc.*, 2019, **141**, 18083–18090.
153 Y. Z. Guo, S. Y. Yan, C. W. Liu, T. F. Chou, J. H. Wang and K. W. Wang, *J. Mater. Chem. A*, 2017, **5**, 14355–14364.
154 L. Gao, Z. Yang, T. Sun, X. Tan, W. Lai, M. Li, J. Kim, Y. F. Lu, S. I. Choi, W. Zhang, C. Ma, S. C. Smith, Y. G. Zhou and H. Huang, *Adv. Energy Mater.*, 2022, **12**, 2103943.
155 D. Chatterjee, S. Shetty, K. Muller-Caspary, T. Grieb, F. F. Krause, M. Schowalter, A. Rosenauer and N. Ravishankar, *Nano Lett.*, 2018, **18**, 1903–1907.
156 Y. Lu, S. Yang, J. Xu, Z. Liu, H. Wang, M. Lin, Y. Wang and H. Chen, *Small*, 2018, **14**, 1801925.
157 Y. Lu, X. Cheng, H. Li, J. Zhao, W. Wang, Y. Wang and H. Chen, *J. Am. Chem. Soc.*, 2020, **142**, 10629–10633.
158 J. L. Yu, H. Jin, Q. Wang, X. L. Wei, H. Y. Chen and Y. W. Wang, *Small*, 2022, 2203458.
159 J. H. Song, Y.-T. Kim, J.-B. Seol, C.-G. Park, J.-M. Myoung and U. Jeong, *Adv. Mater. Interfaces*, 2018, **5**, 1800250.
160 M. Zhu, Q. Shao, Y. Qian and X. Huang, *Nano Energy*, 2019, **56**, 330–337.
161 B. Zhang, X. Zhang, Y. Wei, L. Xia, C. Pi, H. Song, Y. Zheng, B. Gao, J. Fu and P. K. Chu, *J. Alloys Compd.*, 2019, **797**, 1216–1223.
162 Z. Niu, S. Chen, Y. Yu, T. Lei, A. Dehestani, K. Schierle-Arndt and P. Yang, *Nano Res.*, 2020, **13**, 2564–2569.
163 T. Song, F. Gao, L. Jin, Y. Zhang, C. Wang, S. Li, C. Chen and Y. Du, *J. Colloid Interface Sci.*, 2020, **560**, 802–810.
164 Z. Li, Y. Zhang, B. Zou, Z. Wu, F. Gao and Y. Du, *Inorg. Chem.*, 2022, **61**, 9693–9701.
165 H. Xiang, Y. Zheng, Y. Sun, T. Guo, P. Zhang, W. Li, S. Kong, M. Ouzounian, H. Chen, H. Li, T. S. Hu, G. Yu, Y. Feng and S. Liu, *Nanoscale Adv.*, 2020, **2**, 1603–1612.
166 D. Wu and D. Cheng, *Appl. Surf. Sci.*, 2019, **493**, 139–145.
167 C. Zhu, S. Guo and S. Dong, *Adv. Mater.*, 2012, **24**, 2326–2331.
168 L. Jin, Y. Sun, L. Shi, C. Li and Y. Shen, *J. Mater. Chem. B*, 2019, **7**, 4561–4567.
169 S. Y. Ma, H. H. Li, B. C. Hu, X. Cheng, Q. Q. Fu and S. H. Yu, *J. Am. Chem. Soc.*, 2017, **139**, 5890–5895.
170 Q. X. Chen, C. X. Yu, H. H. Li, Z. He and J. W. Liu, *Inorg. Chem.*, 2020, **59**, 1376–1382.
171 C. Li, T. Guo, M. Guo, Y. Song, Z. Nie, X. Li and G. Yu, *J. Phys. Chem. C*, 2022, **126**, 12472–12479.
172 T. Guo, H. Xiang, W. Li, H. Li, H. Chen, S. Liu and G. Yu, *ACS Sustainable Chem. Eng.*, 2020, **8**, 2901–2909.
173 B. Yang, J. Fang, C. Xu, H. Cao, R. Zhang, B. Zhao, M. Huang, X. Wang, H. Lv and R. Che, *Nanomicro Lett.*, 2022, **14**, 170.
174 Z. H. Zhai, Y. Wang, C. H. Si, P. Liu, W. F. Yang, G. H. Cheng and Z. H. Zhang, *Nano Res.*, 2022, DOI: **10.1007/s12274-022-4861-x**.
175 K. R. Sapkota, P. Gyawali, A. Forbes, I. L. Pegg and J. Philip, *J. Appl. Phys.*, 2012, **111**, 123906.
176 Y. Huang, M. Garcia, S. Habib, J. L. Shui, F. T. Wagner, J. L. Zhang, J. Jorne and J. C. M. Li, *J. Mater. Chem. A*, 2014, **2**, 16175–16180.
177 S. N. Zhao, J. F. Huang, Y. Y. Liu, J. H. Shen, H. Wang, X. L. Yang, Y. H. Zhu and C. Z. Li, *J. Mater. Chem. A*, 2017, **5**, 4207–4214.
178 A. Costas, C. Florica, E. Matei, M. E. Toimil-Molares, I. Stavarache, A. Kuncser, V. Kuncser and I. Enculescu, *Beilstein J. Nanotechnol.*, 2018, **9**, 2345–2355.
179 X. T. Deng, S. F. Yin, X. B. Wu, M. Sun, Z. Y. Xie and Q. Z. Huang, *Electrochim. Acta*, 2018, **283**, 987–996.
180 L. Hou, Y. Niu, Y. Jiang, T. Jiao, Y. Guo, Y. Zhou and F. Gao, *Colloids Surf., A*, 2019, **573**, 6–13.
181 Y. Jiang, Y. Guo, Y. Zhou, S. Deng, L. Hou, Y. Niu and T. Jiao, *ACS Omega*, 2020, **5**, 14805–14813.
182 L. Wang, Z. Liu, S. Zhang, M. Li, Y. Zhang, Z. Li and Z. Tang, *Int. J. Hydrogen Energy*, 2021, **46**, 8549–8556.
183 D. Song, Y. Li, X. Lu, M. Sun, H. Liu, G. Yu and F. Gao, *Anal. Chim. Acta*, 2017, **982**, 168–175.
184 C. Santoro, P. Bollella, B. Erable, P. Atanassov and D. Pant, *Nat. Catal.*, 2022, **5**, 473–484.
185 X. Q. Wang, Z. J. Li, Y. T. Qu, T. W. Yuan, W. Y. Wang, Y. Wu and Y. D. Li, *Chem*, 2019, **5**, 1486–1511.
186 K. Wang, H. Yang, J. Zhang, G. Ren, T. Cheng, Y. Xu and X. Huang, *Nano Res.*, 2022, **15**, 5865–5872.
187 Z. J. Liu, J. Qi, M. X. Liu, S. M. Zhang, Q. K. Fan, H. P. Liu, K. Liu, H. Q. Zheng, Y. D. Yin and C. B. Gao, *Angew. Chem., Int. Ed.*, 2018, **57**, 11678–11682.
188 J. J. Wang, X. P. Li, B. F. Cui, Z. Zhang, X. F. Hu, J. Ding, Y. D. Deng, X. P. Han and W. B. Hu, *Rare Met.*, 2021, **40**, 3019–3037.
189 H. Xie, T. Y. Wang, J. S. Liang, Q. Li and S. H. Sun, *Nano Today*, 2018, **21**, 41–54.
190 P. Saha, S. Amanullah and A. Dey, *Acc. Chem. Res.*, 2022, **55**, 134–144.
191 J. Yu, W. Wang, S. Li, B. Yu, H. Chen and Y. Wang, *Chem. Commun.*, 2022, **58**, 989–992.
192 S. Zhu, Q. Wang, X. Qin, M. Gu, R. Tao, B. P. Lee, L. Zhang, Y. Yao, T. Li and M. Shao, *Adv. Energy Mater.*, 2018, **8**, 1802238.

193 N. Han, M. Z. Sun, Y. Zhou, J. Xu, C. Cheng, R. Zhou, L. Zhang, J. Luo, B. L. Huang and Y. G. Li, *Adv. Mater.*, 2021, **33**, 2005821.
194 Y. J. Sun, M. C. Luo, Y. N. Qin, S. H. Zhu, Y. J. Li, N. Y. Xu, X. X. Meng, Q. S. Ren, L. Wang and S. J. Guo, *ACS Appl. Mater. Interfaces*, 2017, **9**, 34715–34721.
195 X. X. Xu, H. Lv, L. Z. Sun, P. Song, B. Liu and X. Chen, *ChemPlusChem*, 2020, **85**, 970–976.
196 W. L. Wu, J. W. Li, Z. Y. Chen, W. Z. Chen, H. S. Pang, K. B. Ma and J. Zeng, *J. Catal.*, 2019, **373**, 209–214.
197 L. Fu, C. Yang, R. Wei, X. Pei, J. Teng, D. Kong, Y. Lu, Y. Guo, T. Liu, Y. Hu, B. Yin, Z. Zhang, A. Li, L. Wang and X. Han, *Mater. Today Nano*, 2021, **15**, 9.
198 H. Cheng, N. Yang, Q. Lu, Z. Zhang and H. Zhang, *Adv. Mater.*, 2018, **30**, 1707189.
199 Y. Chen, Z. Lai, X. Zhang, Z. Fan, Q. He, C. Tan and H. Zhang, *Nat. Rev. Chem.*, 2020, **4**, 243–256.